united nations
educational, scientific
and cultural
organization

international atomic
energy agency

the
abdus salam
international centre for theoretical physics

SMR 1232 - 39

XII WORKSHOP ON
STRONGLY CORRELATED ELECTRON SYSTEMS

17 - 28 July 2000

SOME NEW PHYSICS OF ORGANIC SEMICONDUCTORS

B. BATLOGG
Bell Laboratories, Lucent Technologies
NJ-07974 Murray Hill, U.S.A.

These are preliminary lecture notes, intended only for distribution to participants.

Some new physics of organic semiconductors

B. Batlogg, J.H. Schön, and Ch. Kloc

Bell Labs, Lucent Technologies
Murray Hill, NJ

ictp
17-28 July 2000

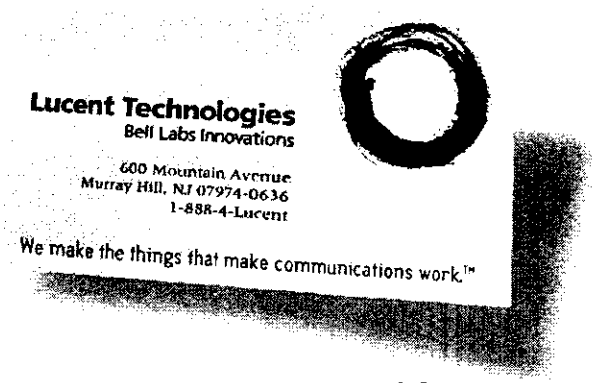

S. Frolov, S. Berg, G.A. Thomas, B. Crone, A. Dodabalapur, Z. Bao, H. Katz, ...

Practical aspects of charge transport

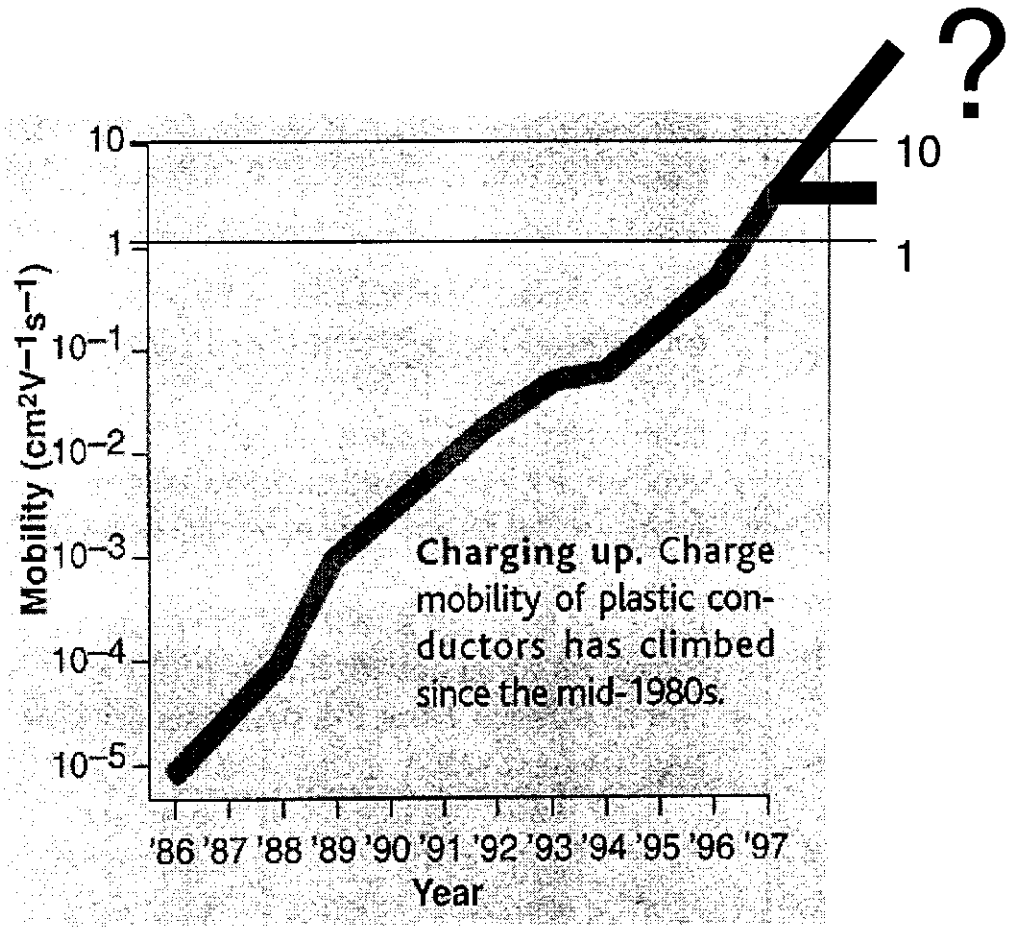

From A. Hellemans, Science 283,771, 5Feb.1999

48-stage shift register

B. Crone, A. Dodabalapur et. al. 2000

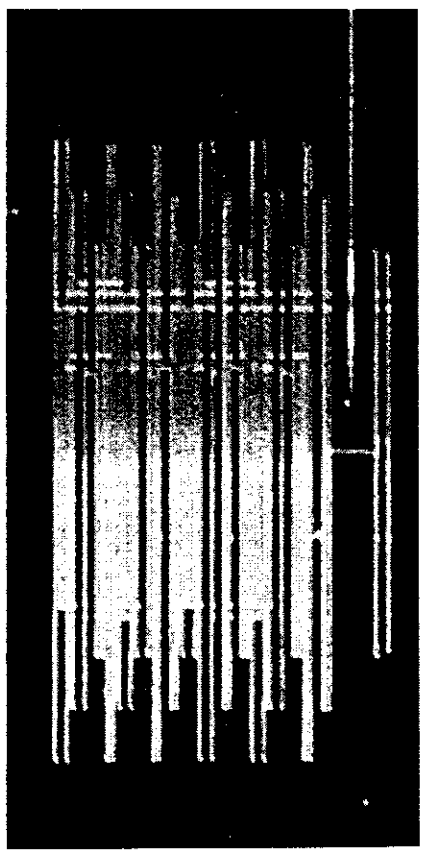

Today's program

- Measurements and materials
- Carrier mobilitiy
  - oligothiophene and polyacene crystals
  - orientation, temperature
  - non-linear transport (velocity saturation, ...)
- Interpretation (coherent bandwidth, ...)
- Physical phenomena in high-mobility crystals
- Device exploration
  - thin film and bulk FETs
  - photovoltaic cells
  - most recent developments (injection laser)

2D "M-I-T"
Quantum Hall Transport
gate-induced superconductivity
in C_{60}, Ac, Tc, Pc

Typical packing of molecules

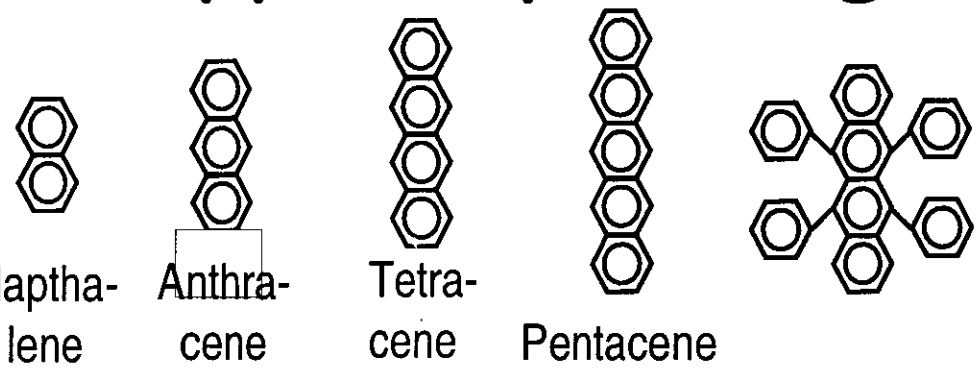

Naptha-lene | Anthra-cene | Tetra-cene | Pentacene

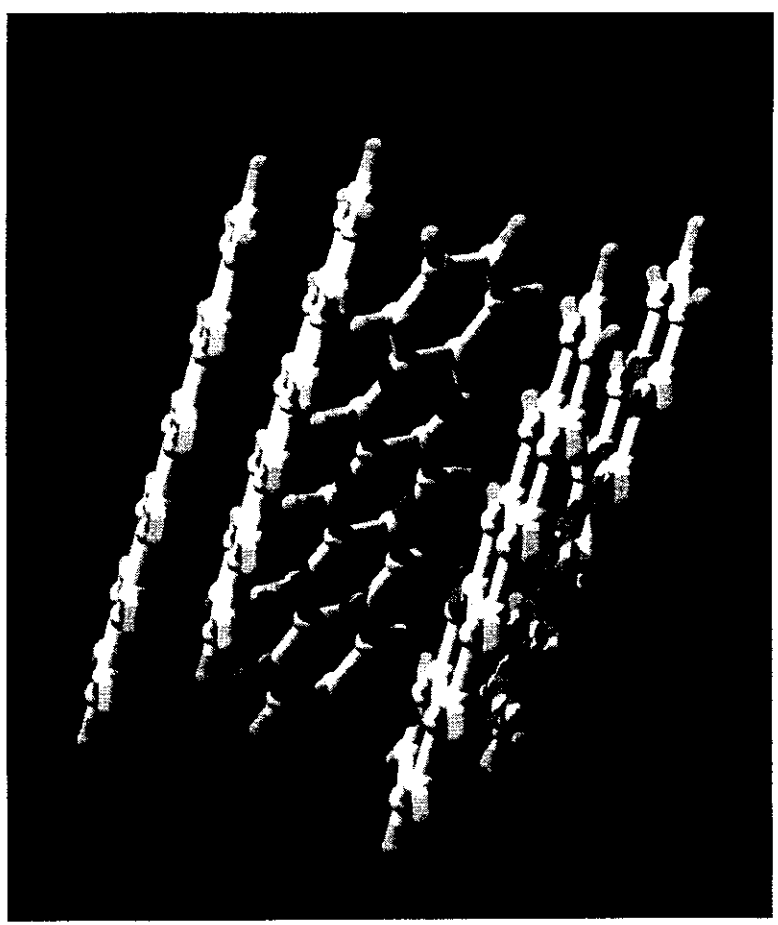

Example: pentacene

Triclinic lattice

Herringbone packing

Layered structure

Charge transport
due to π-π^* overlap

Possible high mobility

Molecules pack in layers

Side view

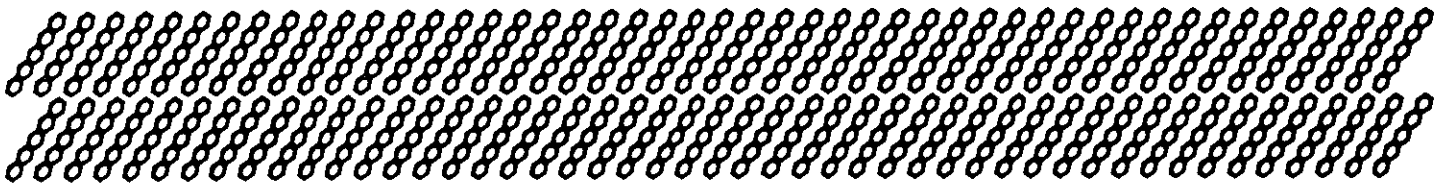

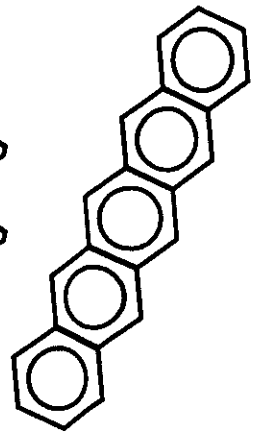

weak bonding between molecules (van der Waals)
- no broken bonds
- no surface states

Charge transport due to π-π^* overlap

Naphtalene

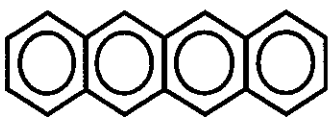

Tetracene

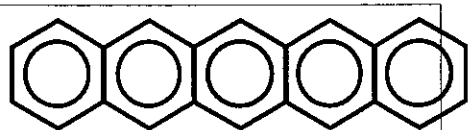

Pentacene

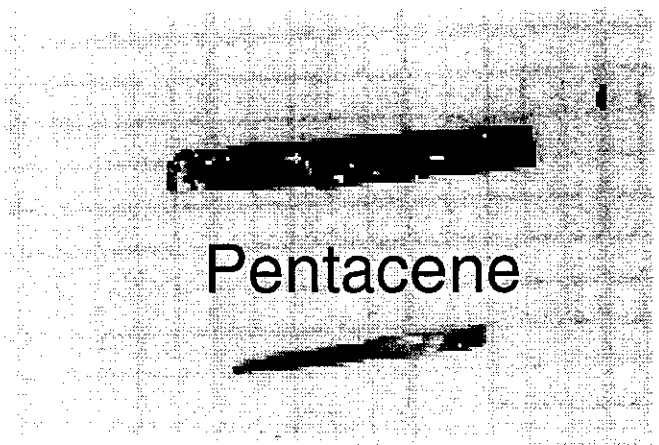

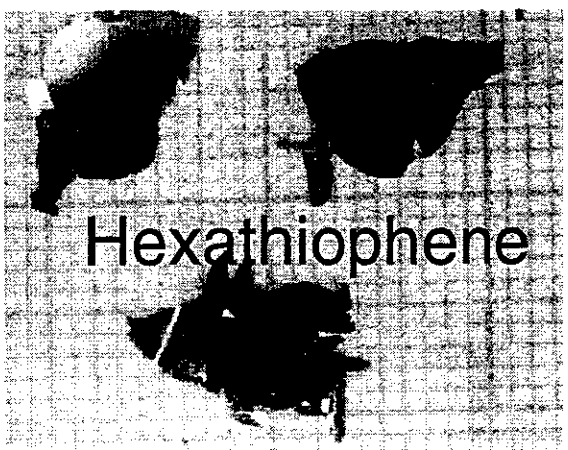

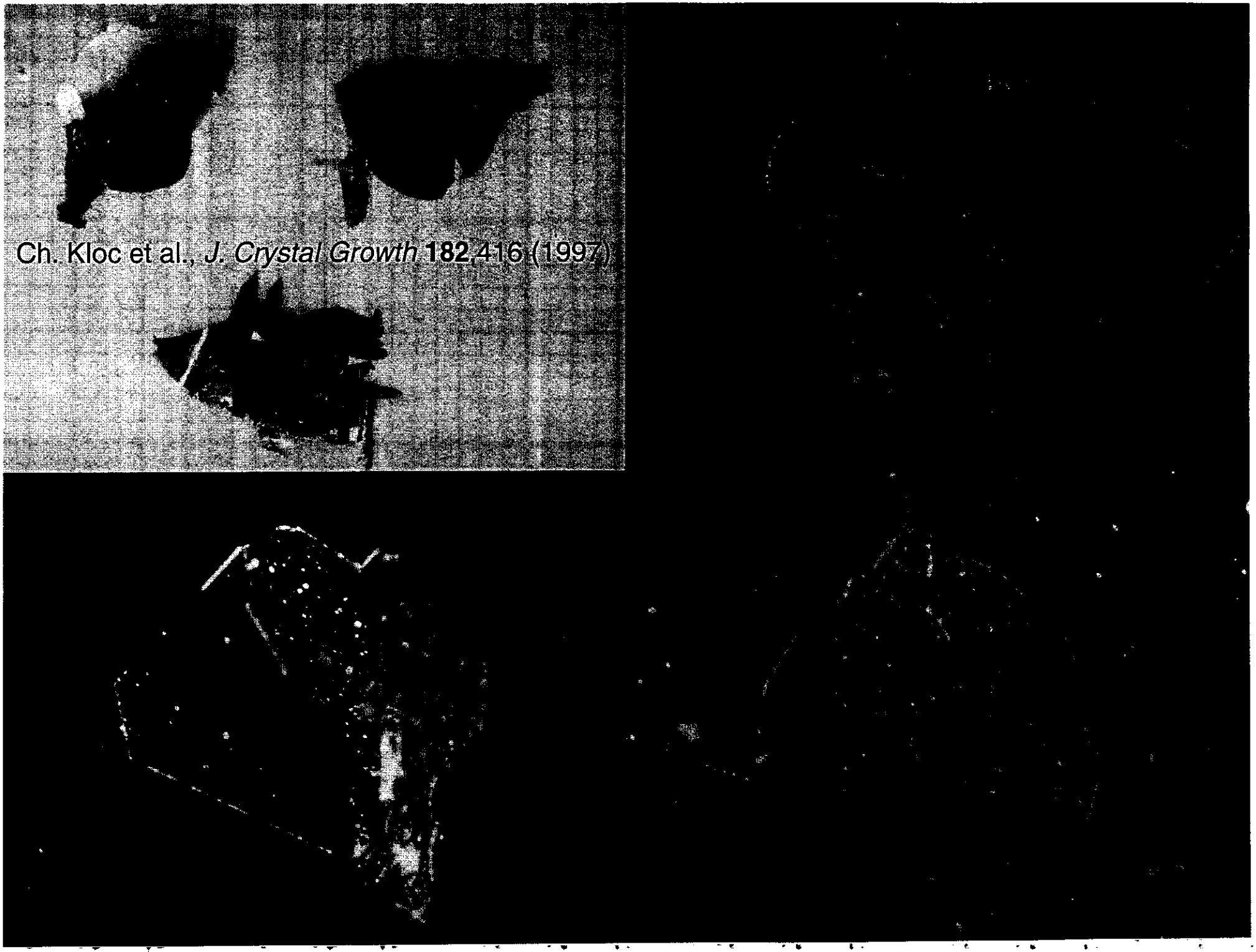
Ch. Kloc et al., *J. Crystal Growth* **182**,416 (1997)

Silicon ↔ organic molecular crystals

Crystal Structure-Electronic Structure

4T high temperature phase

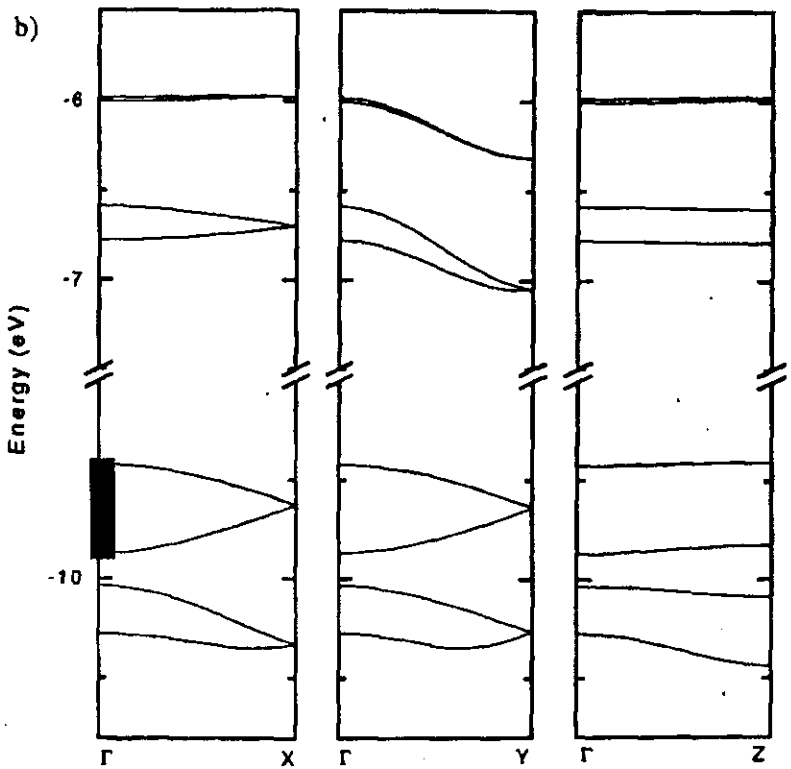

Measured mobility : 0.15 cm^2/Vs

T. Siegrist et al., Adv. Mater. 10, 379 (1998)

Typical (im)purity levels

Compound	Acceptors (cm^{-3})	Traps (cm^{-3})
6T (LT)	9.10^{10}	9.10^{14}
6T (HT)	7.10^{10}	7.10^{14}
anthradithiophene	$\sim 10^{11}$	4.10^{14}
pentacene	$\sim 10^{10}$	3.10^{13}

Velocity saturation due to non-parabolic bands (?)

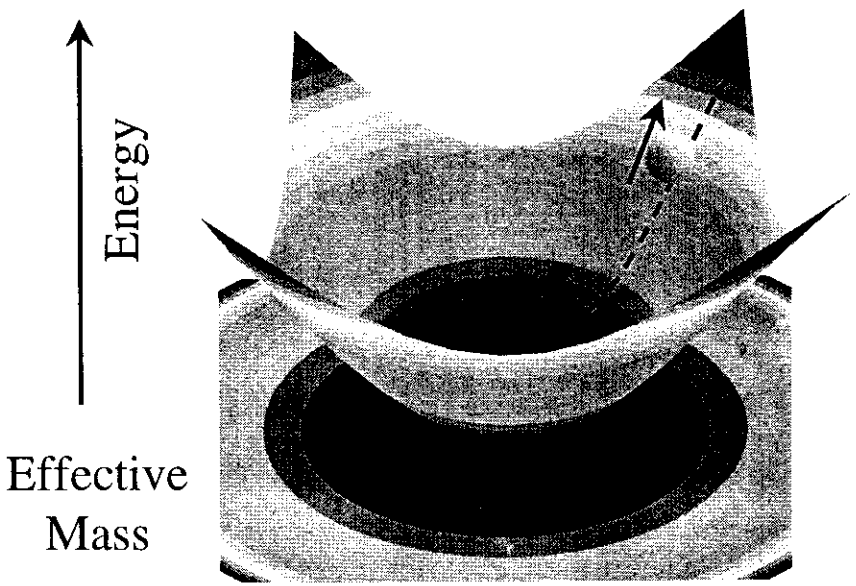

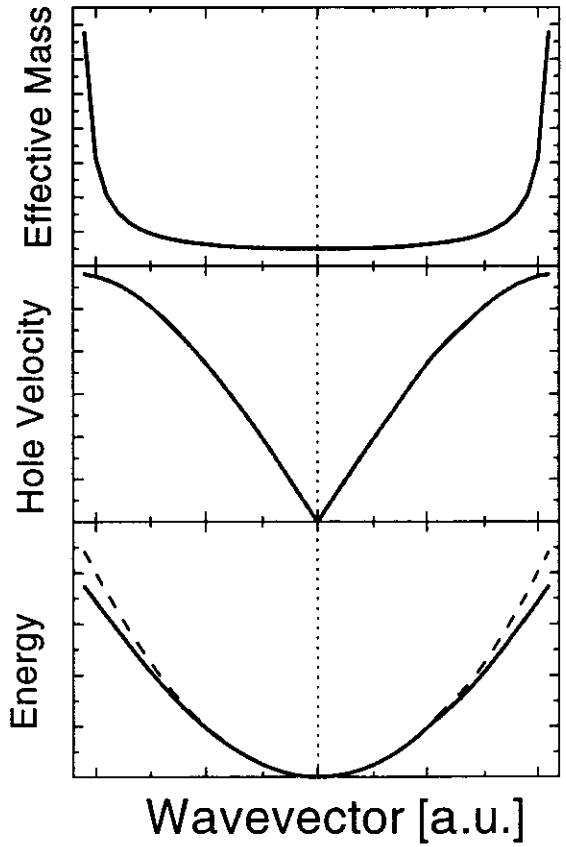

$$v_{h,s} \propto W$$

$$W \propto \exp\left(-g^2\left(n+1/2\right)\right)$$

$$n = \left(\exp\left(\frac{\blacksquare}{k_B T}\right) - 1\right)^{-1}$$

Non-linear transport

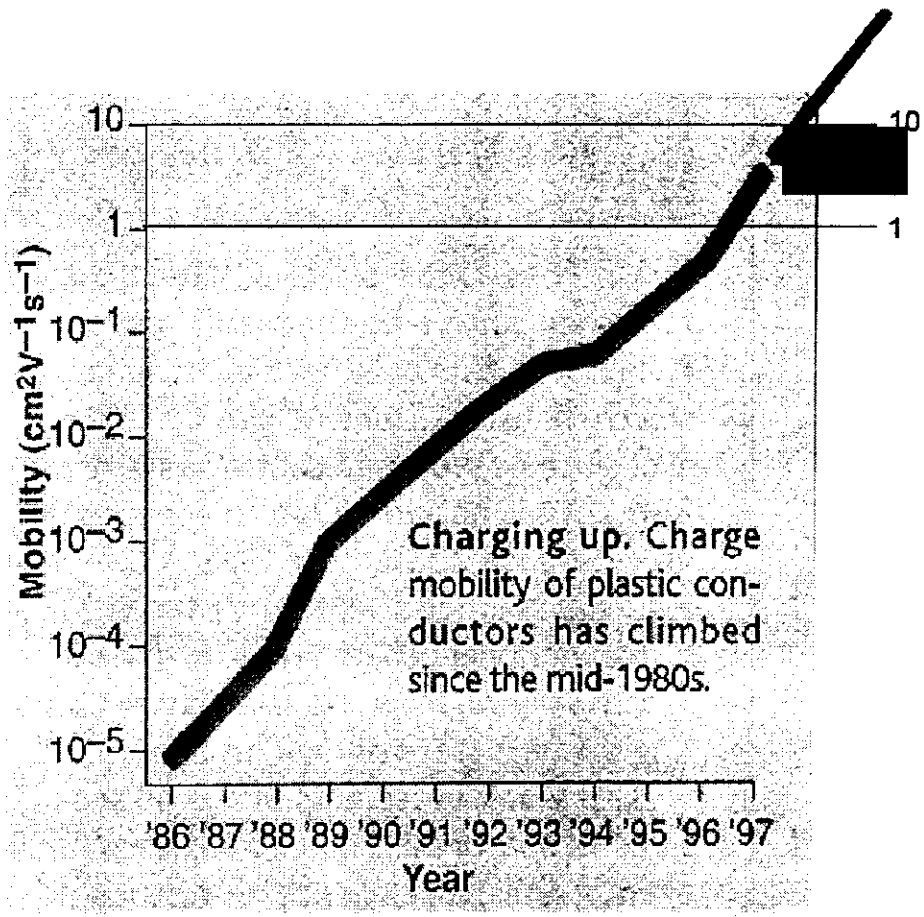

From A. Hellemans, Science 283,771, 5Feb.1999

Limit for Hydrocarbons:
around 3-10 cm^2/Vs

Search for New Transport Mechanisms

Different Stacking Geometry
Charge Transfer Salts
Partly Covalent Bonds
Low Dimensional Systems
...

Ambipolar transport in Pc and in C_{60}

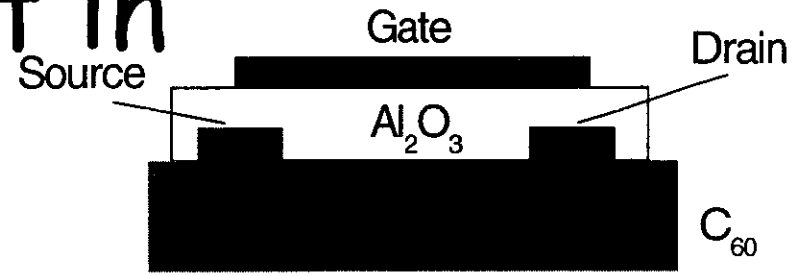

p - channel

Ambipolar transport

n - channel

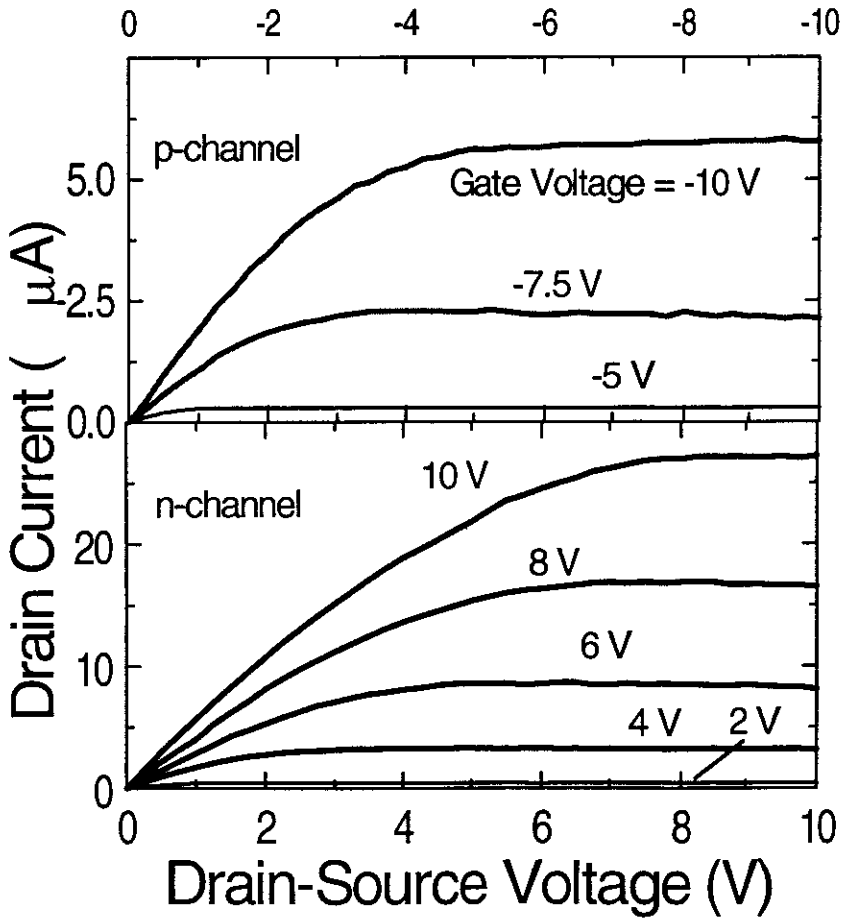

Science **287**,1022-1023 (2000)
11 February 2000

Lucent Technologies
Bell Labs Innovations

Ambipolar Transistor Materials

	P (cm^2/Vs)	N (cm^2/Vs)
Pentacene	3.1	2.2
Tetracene	2.7	2.0
Anthracene	2.5	1.8
Perylene	0.5	5.5
α6T	1.1	0.7
α4T	0.4	0.2
C_{60}	2.1	1.8

J.H. Schön et al. Proc. EMRS 2000
Proc MRS '99

High Quality Organic Molecular Crystals

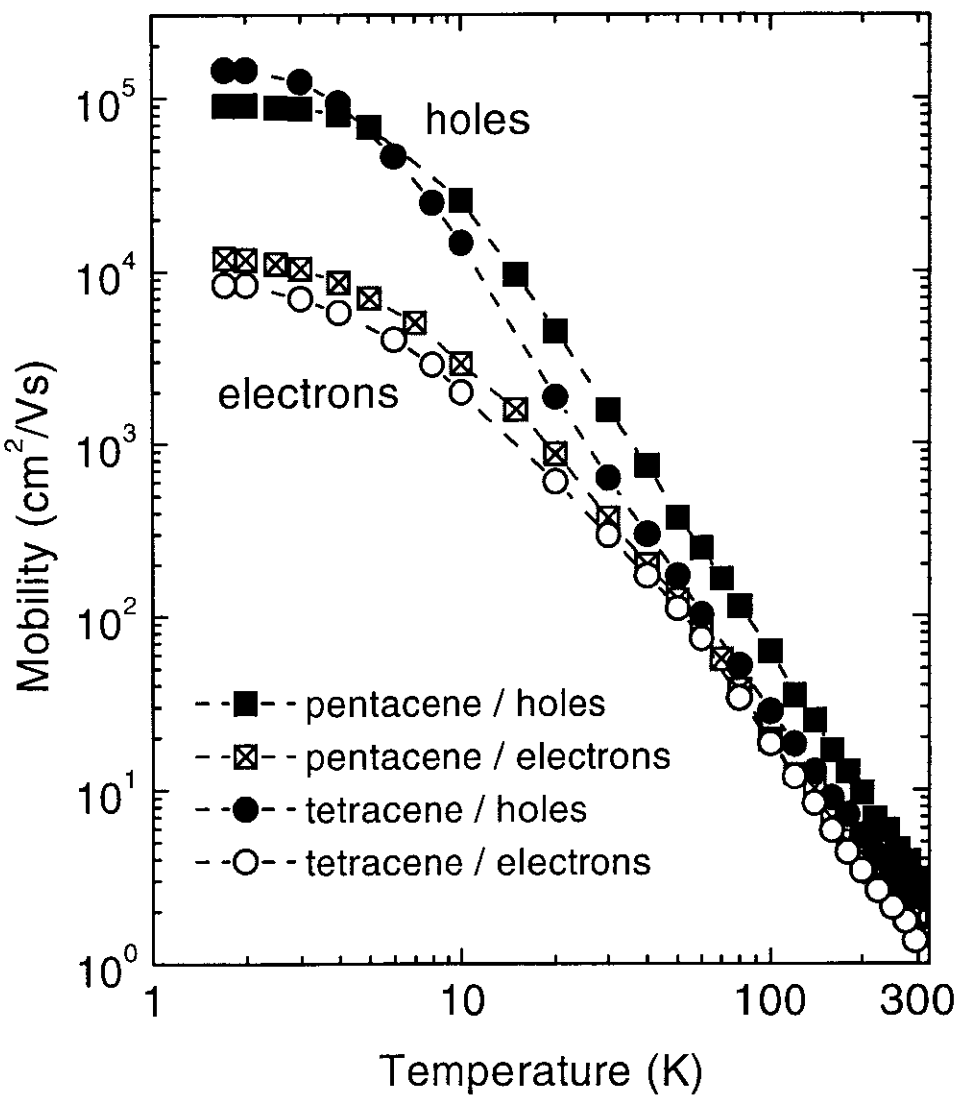

~ 10^{10} cm^{-3} acceptors
3.10^{13} cm^{-3} deep traps

Carrier scattering rates lower than in most inorganic semiconductors, except MBE modulation doped GaAs

$\mu = e\,\tau / m^*$
$m^* = 1.5 m_e$

Q H transport for electrons and holes in Pc

(Gate sweep)

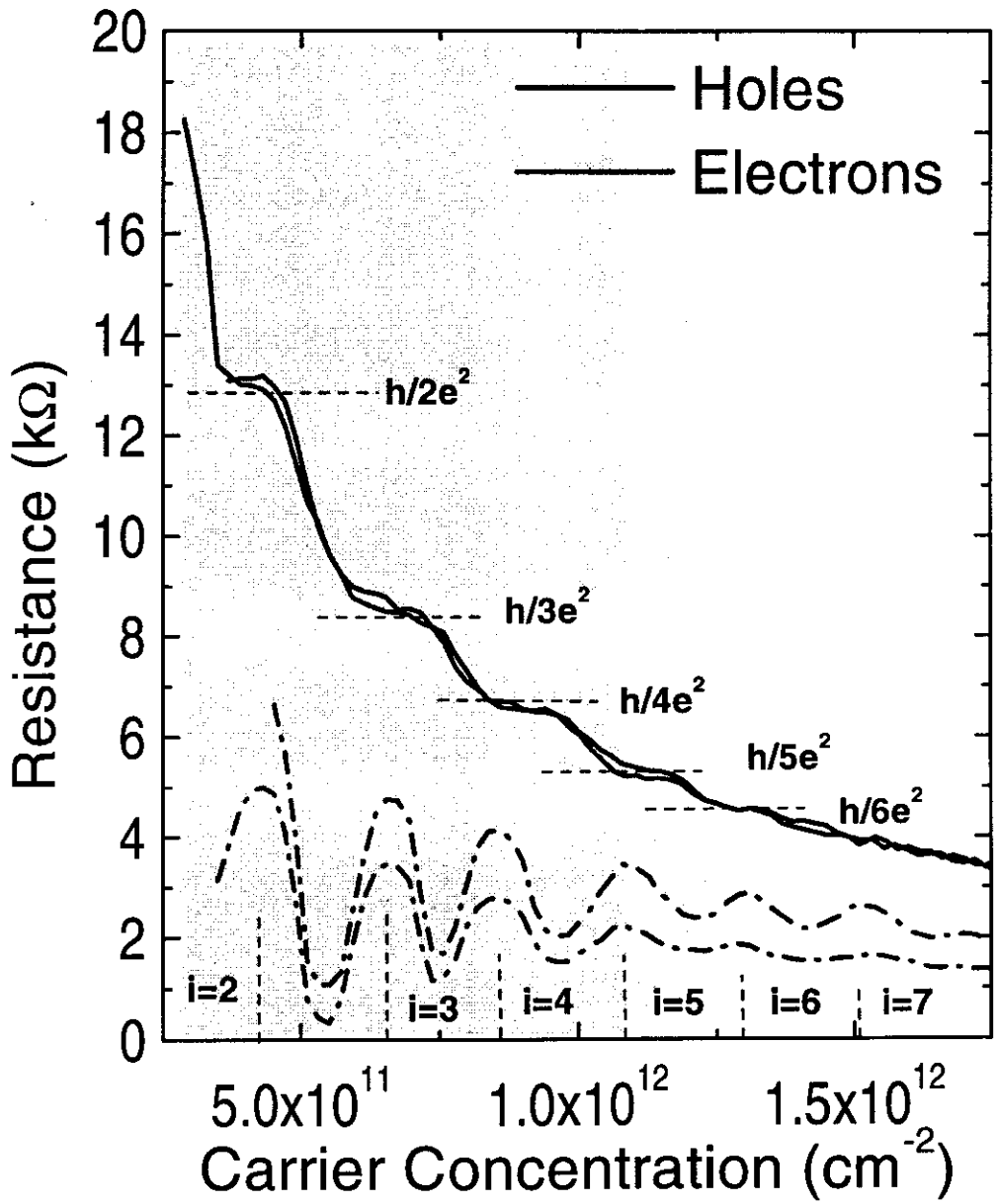

H. Schön et al.
Science **288**, 2338-2340 (2000)
30 June 2000

Quantum Hall effect in Pc

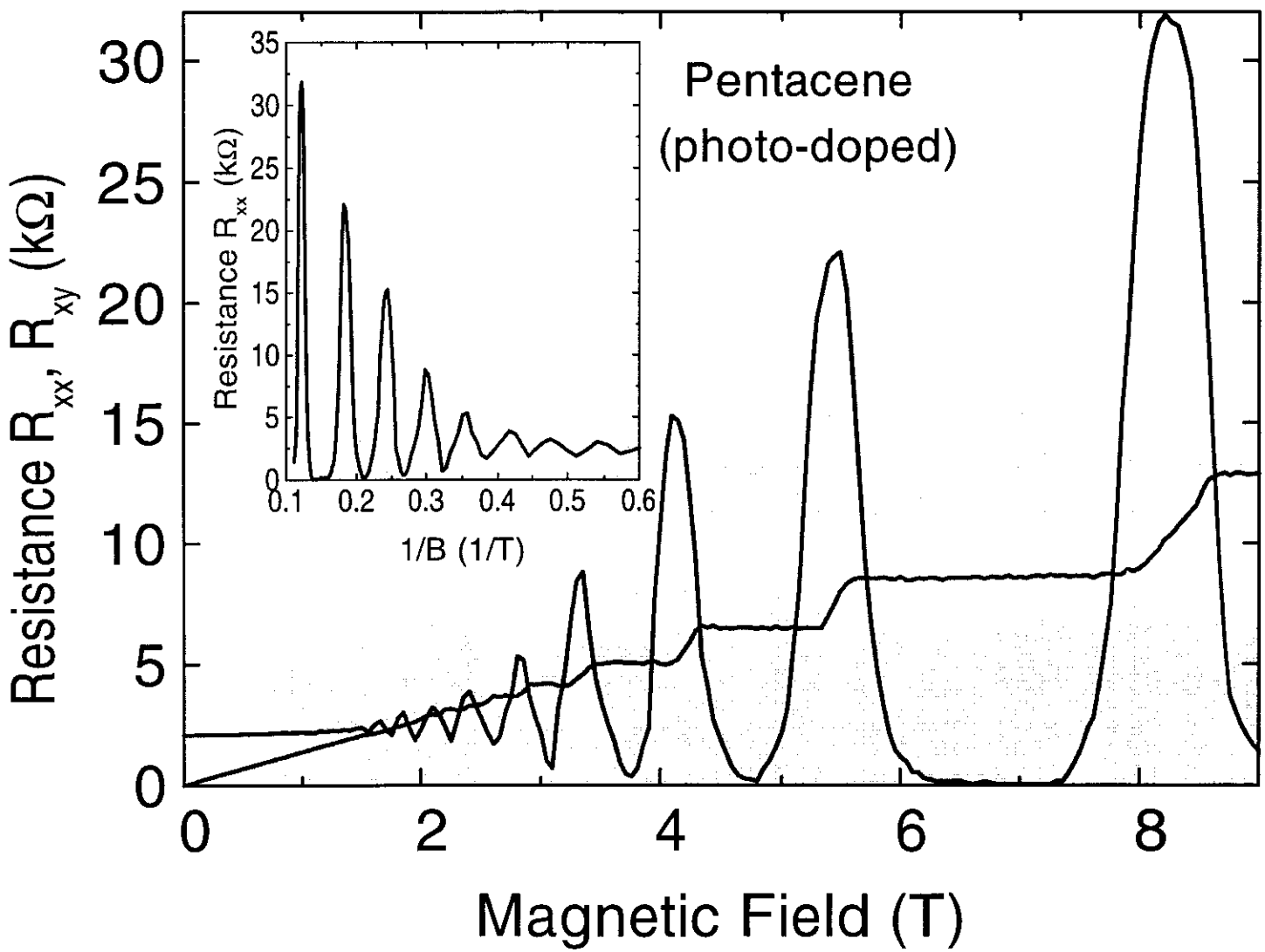

Lucent Technologies
Bell Labs Innovations

Effective mass from S-dH osc.

$m_{eff} = 1.55\ m_e$

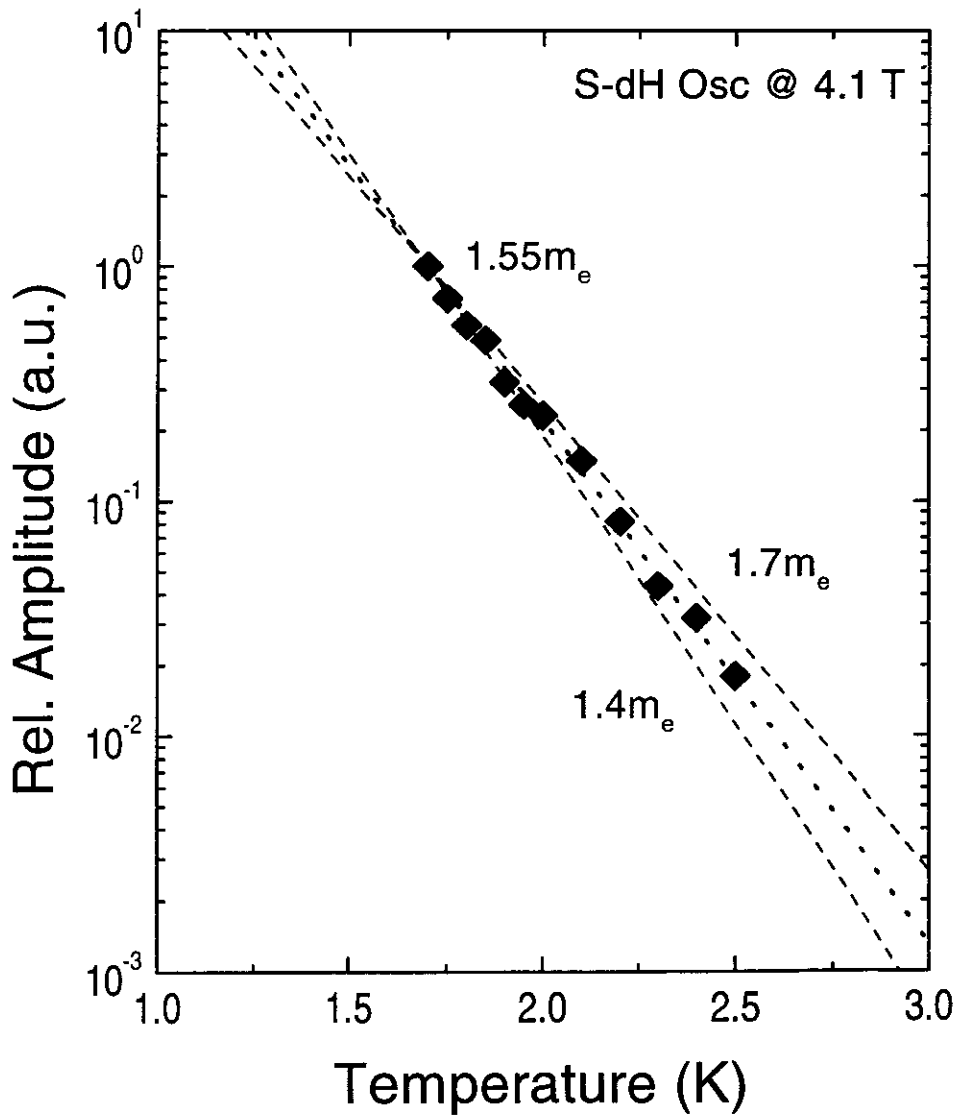

Quantum Hall transport in 2D hole gas

Integral QHE

Tetracene at T=1.7 K

Fractional QHE

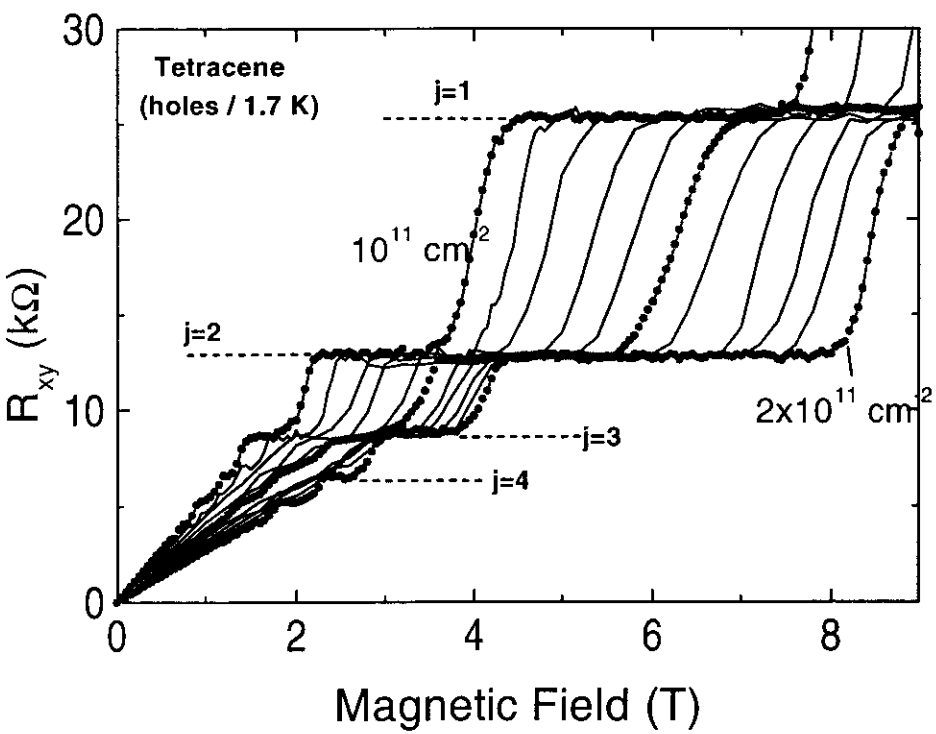

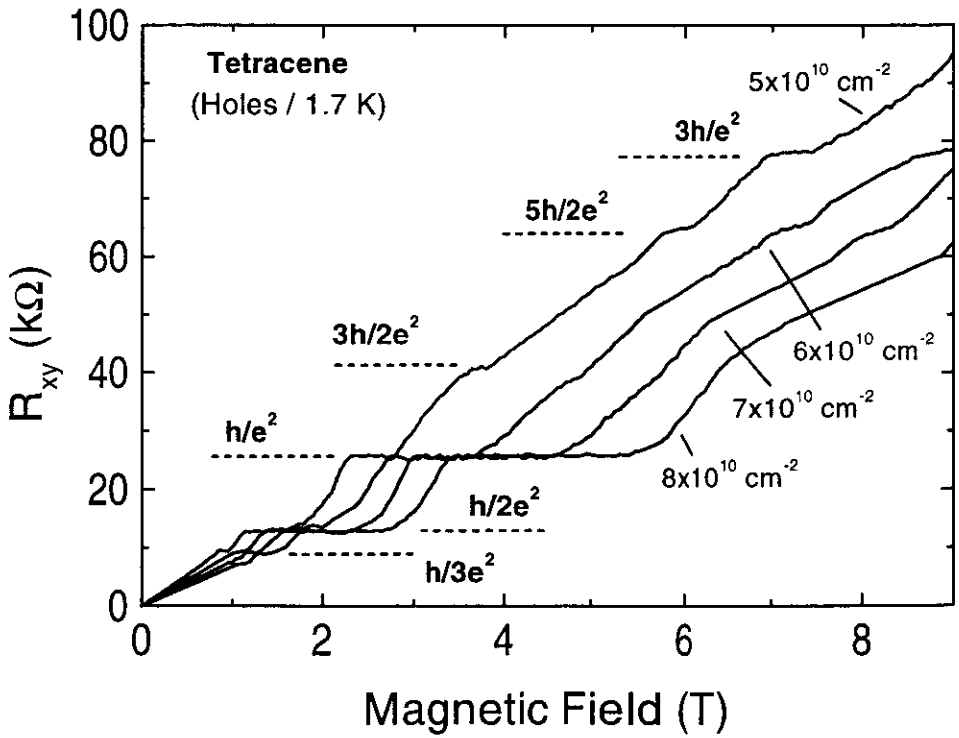

Gate-induced superconductivity in C_{60} crystals

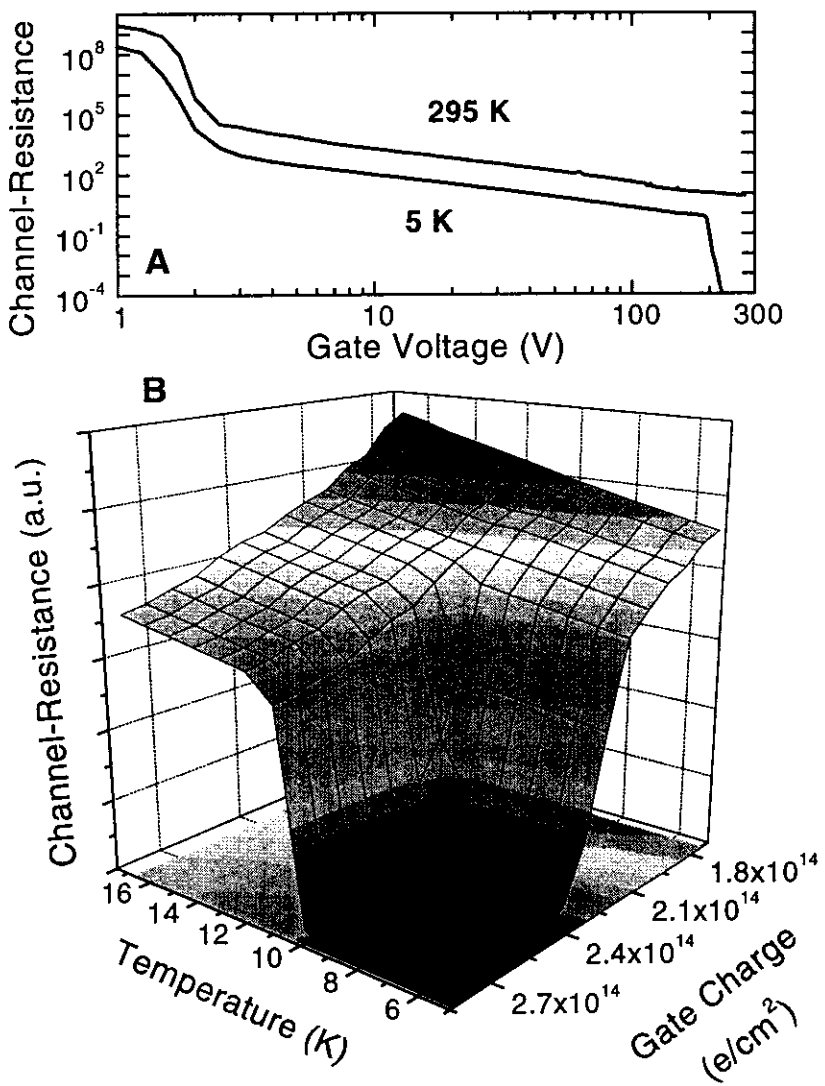

Science **288**,656 (2000)
28 April 2000

Lucent Technologies
Bell Labs Innovations

Gate-induced superconductivity in C_{60}

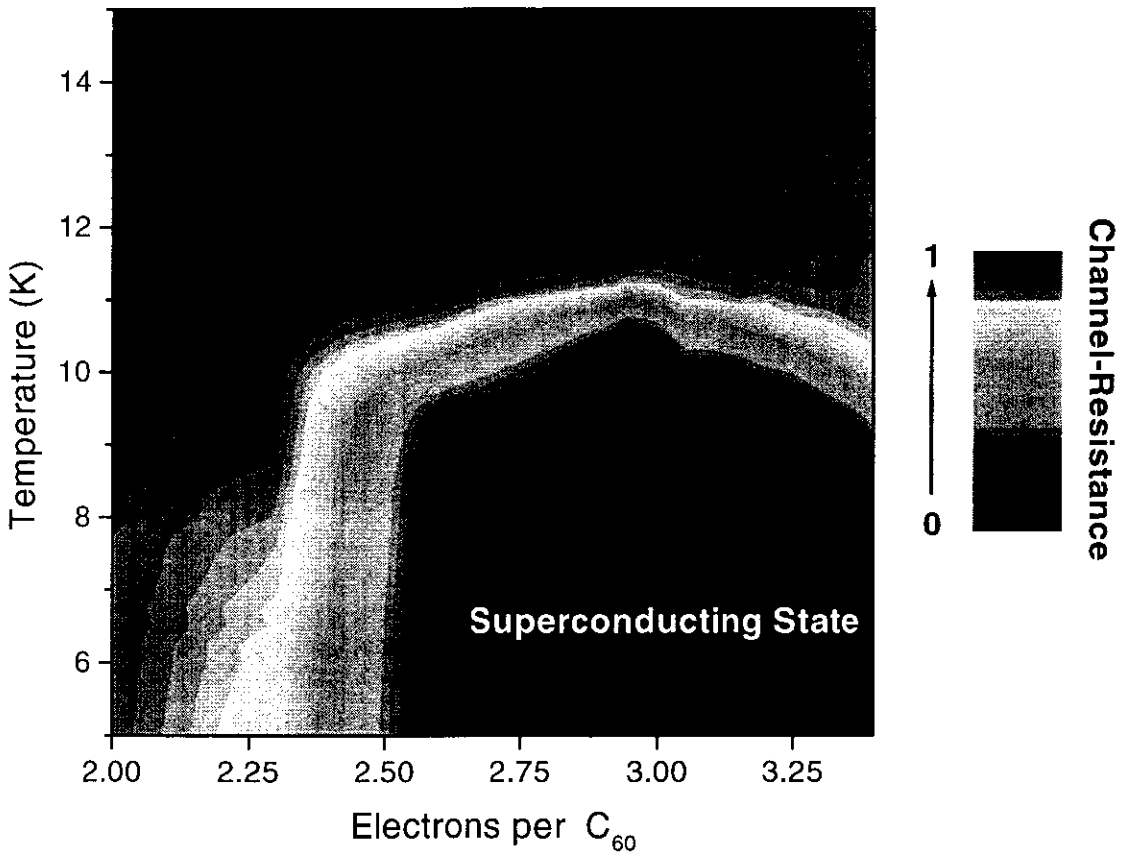

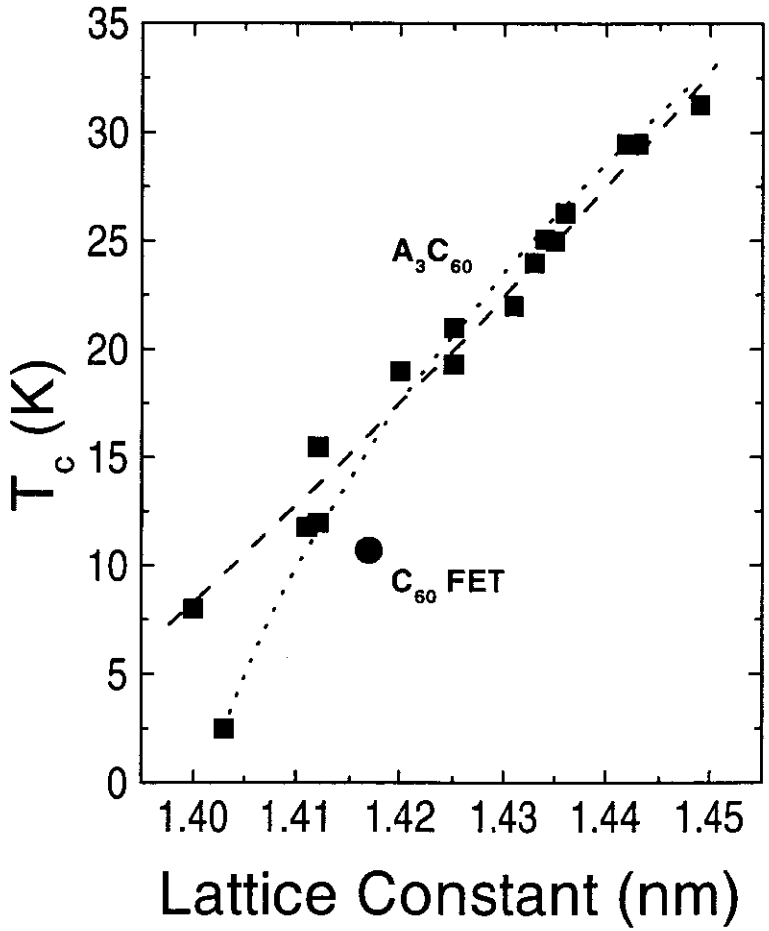

Metallic Pentacene

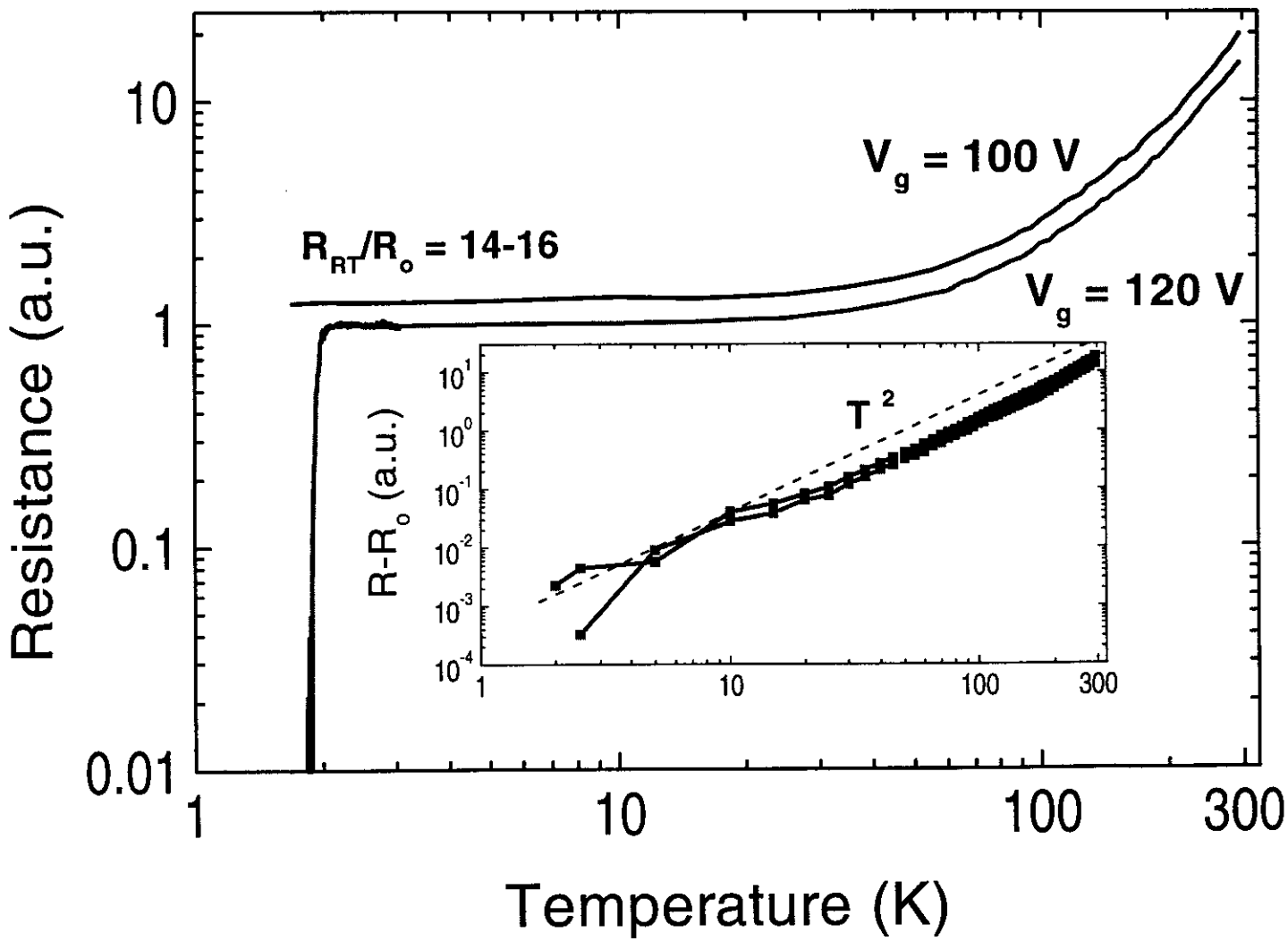

To appear in
Nature, July/Aug. 2000

Gate-induced superconductivity in Ac, Tc and Pc

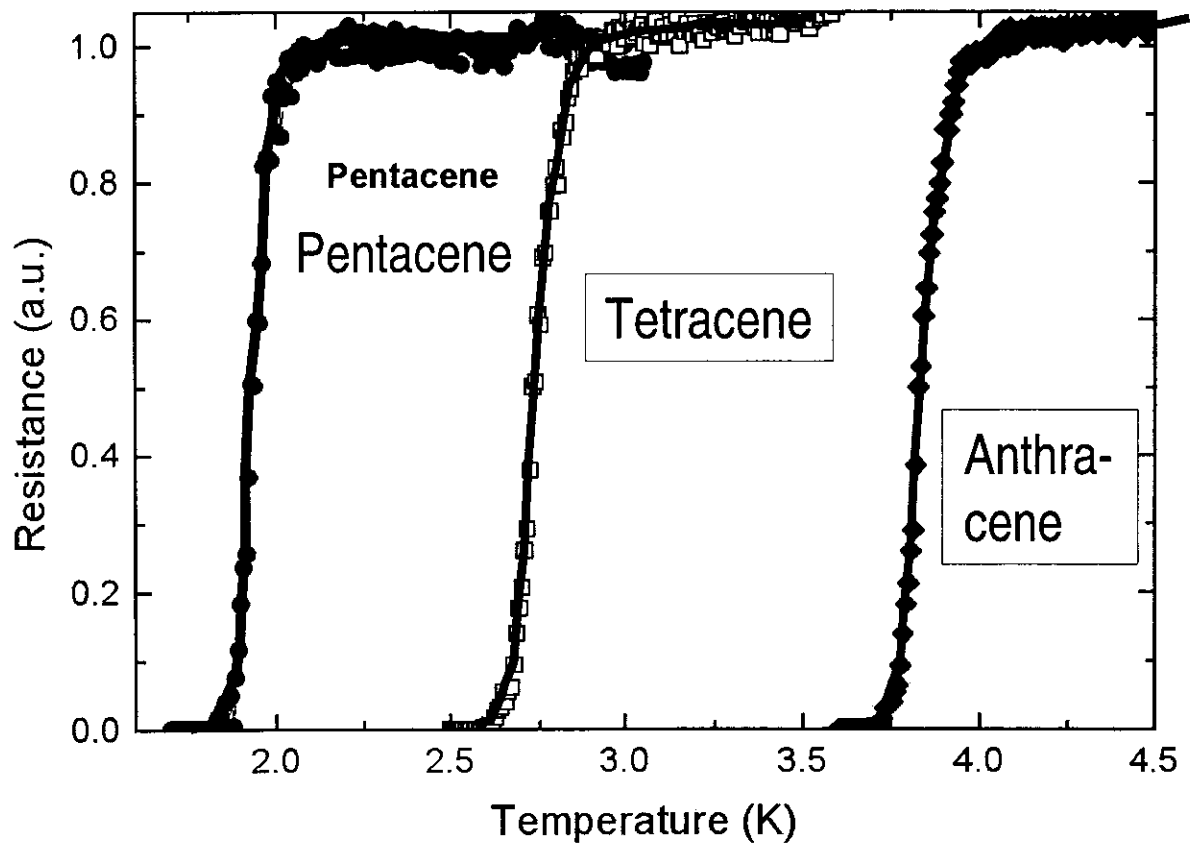

To appear in
nature July 2000

Superconductivity in Pentacene

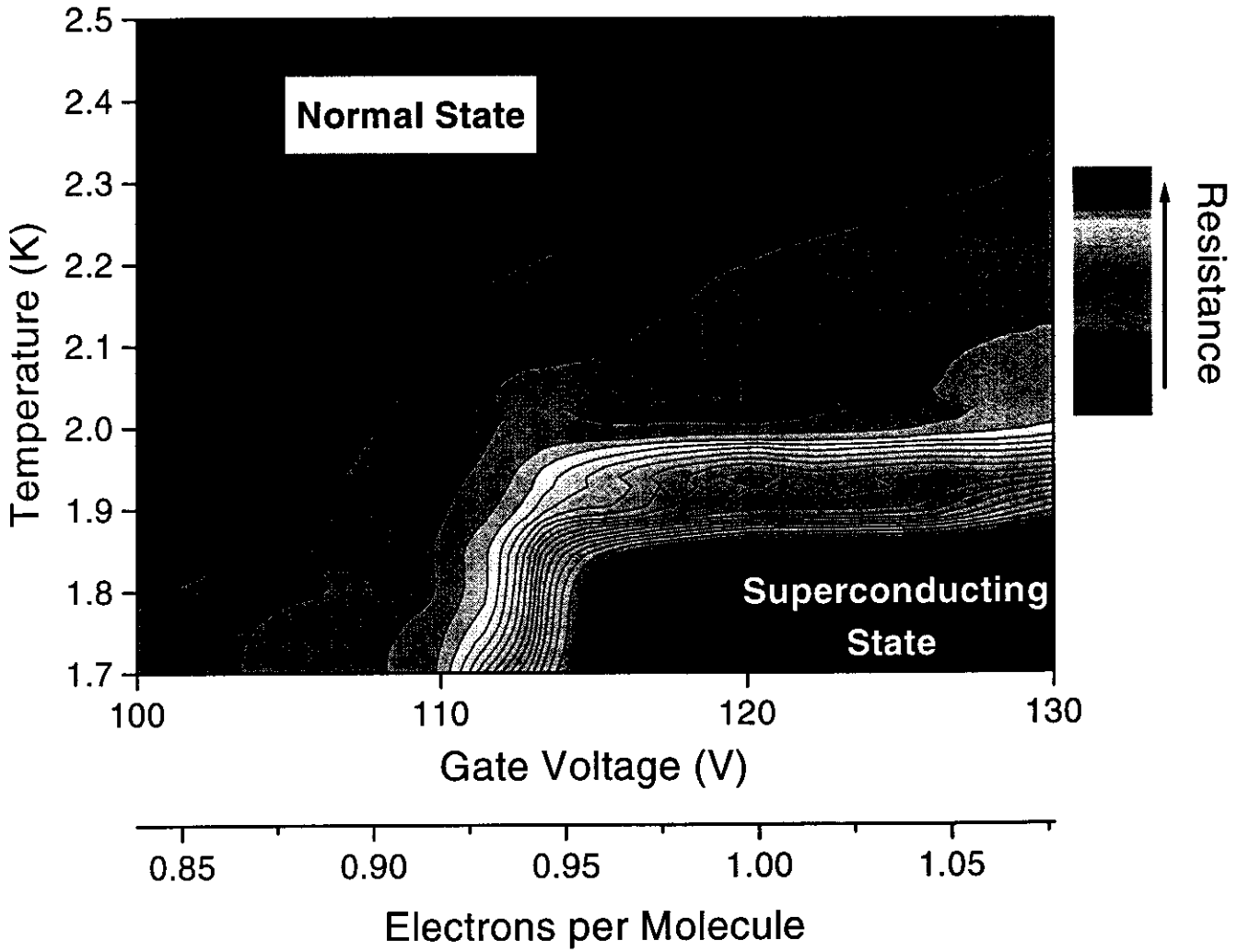

To appear in
Nature, July/August 2000

Ambipolar Pentacene Field-Effect Transistors and Inverters

J. H. Schön,* S. Berg, Ch. Kloc, B. Batlogg

Organic field-effect transistors based on pentacene single crystals, prepared with an amorphous aluminum oxide gate insulator, are capable of ambipolar operation and can be used for the preparation of complementary inverter circuits. The field-effect mobilities of carriers in these transistors increase from 2.7 and 1.7 square centimeters per volt per second at room temperature up to 1200 and 320 square centimeters per volt per second at low temperatures for hole and electron transport, respectively, following a power-law dependence. The possible simplification of the fabrication process of complementary logic circuits with these transistors, together with the high carrier mobilities, may be seen as another step toward applications of plastic electronics.

Organic thin-film field-effect transistors (FETs) have been studied extensively throughout the last decade, and tremendous progress in performance of these devices has been achieved (*1–4*). Among these organic materials, pentacene has been found to have the highest mobilities for hole transport (p channel) (*5*, *6*). State-of-the-art organic thin-film transistors reach performances similar to those of devices prepared from hydrogenated amorphous silicon (a-Si:H), with mobilities around 1 $cm^2\ V^{-1}\ s^{-1}$ and on/off ratios surpassing 10^6, and with the use of high–dielectric constant gate insulators, operating voltages as low as 5 V can be achieved (*7*). These accomplishments demonstrate that the use of organic electronic devices may become feasible and desirable in areas in which large area coverage, mechanical flexibility, low-temperature processing, and overall low cost are required. Potential applications include low-end data storage, such as identification tags or smart cards (*8*), and even switching devices for active displays (*9*), especially because the integration of organic FETs and organic light-emitting diodes into smart pixels has been demonstrated (*9–11*). However, organic FETs have worked only as unipolar devices in accumulation or depletion, never in inversion. To exploit advantages of complementary logic, such as low-power dissipation, good noise margins, robust operation, and ease of circuit design, two different organic materials have to be used. The different semiconductors can be embedded into one heterostructure device (*12*, *13*) or into many separate devices (*14–17*), leading to all-organic digital circuits. The limitation of charge transport by only one carrier type is generally ascribed to effective trapping of the other carrier in the material itself as well as at the interface to the gate dielectric (*12*, *13*). Therefore, the use of ultrapure, high-quality materials seems to be a prerequisite to overcome this limitation.

Here, we report on organic FETs based on pentacene single crystals working as ambipolar devices both in accumulation (p type) and inversion (n type). High-purity pentacene single crystals were grown by physical vapor transport in a stream of hydrogen (*18*). Space-charge–limited current measurements (*19*) revealed trap concentrations (for holes) and acceptor densities as low as 10^{13} and 10^{11} cm^{-3}, respectively. Gold source and drain contacts (thickness of 50 nm) were evaporated through a shadow mask, defining a channel length between 25 and 50 μm and a width of 500 to 1500 μm. Al_2O_3 was deposited as gate dielectric layer by radio frequency–magnetron sputtering (capacitance $C_i \approx$ 30 nF cm^{-2}; thickness of 250 nm). Finally, the gate electrode (thickness of 100 nm) was prepared by thermal evaporation of gold (Fig. 1).

Typical device characteristics at room temperature of a pentacene single-crystal FET (Fig. 2) show the device working in both accumulation and inversion modes. The device operation of organic transistors is well described by standard FET equations (*20*), as previously shown (*7*). For accumulation (hole transport), the mobility is 2.7 $cm^2\ V^{-1}\ s^{-1}$, and the on/off ratio at 10 V is 10^9. Typical threshold voltages are in the range of −1 V. In combination with the steep subthreshold slope of 200 meV per decade (Fig. 3), this low threshold voltage indicates the high quality of the pentacene single crystal as well as the pentacene-Al_2O_3 interface. An electron mobility of 1.7 $cm^2\ V^{-1}\ s^{-1}$ and an on/off ratio of 10^8 are measured for operation in inversion. The higher threshold voltage of about 5 V reveals a higher density of traps for electrons than for holes. Nevertheless, n-channel transport can be obtained in pentacene devices. The observed field-effect mobility is similar to previous time-of-flight mobilities measured on related compounds such as naphtalene or anthracene (*21*).

Because no organic material has to be patterned, the use of ambipolar devices can substantially simplify the fabrication of complementary metal oxide semiconductor (CMOS)–

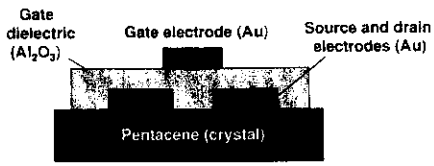

Fig. 1. Schematic structure of the FETs based on single crystalline pentacene. Gold and Al_2O_3 were used as electrode and gate insulator materials, respectively.

Bell Laboratories, Lucent Technologies, Mountain Avenue, Murray Hill, NJ 07974, USA.

*To whom correspondence should be addressed. E-mail: hendrik@lucent.com

23

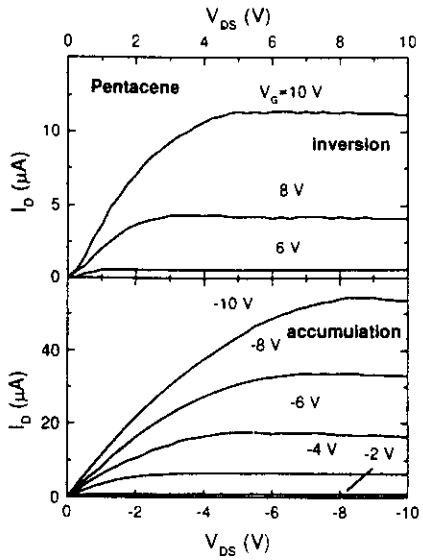

Fig. 2. Drain current (I_D) versus drain-source voltage (V_{DS}) characteristics at room temperature of a pentacene single-crystal transistor in inversion mode (n type, top) and accumulation mode (p type, bottom). V_G, gate voltage.

like circuits. Complementary circuits in which single transistors operate either as n- or p-channel device have been proposed and analyzed for a-Si:H–based FETs (*22*, *23*). From the transfer characteristic of a CMOS-like inverter circuit based on ambipolar pentacene FETs (Fig. 4), a gain as high as 10 has been measured. Moreover, inverters with a gain as high as 23 have been prepared with different metals as source and drain electrodes for n- and p-channel operation. Because of the high mobilities observed in the present devices, especially for n-type transport, a substantial improvement of switching speed (*15*, *17*) and performance of organic complementary circuits can be expected from the use of ambipolar transistors in addition to the simplification of processing.

The high quality of the pentacene single crystals and of the pentacene-Al_2O_3 interface opens up possibilities for studying the physics

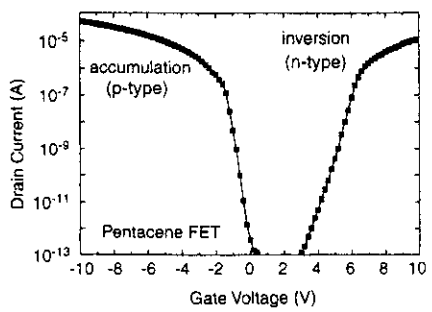

Fig. 3. Drain current versus gate voltage characteristics at room temperature of a pentacene single-crystal transistor. The on/off current ratio ($|V_{DS}|$ = 10 V) is 10^8 and 10^9 for n- and p-channel operation, respectively.

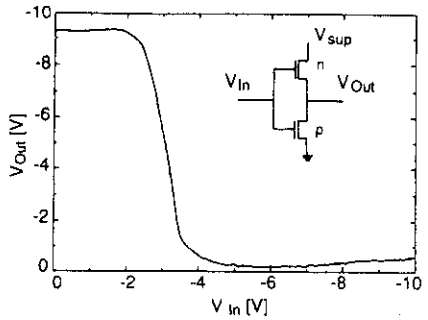

Fig. 4. Transfer characteristic of a CMOS-like ambipolar pentacene inverter circuit (see inset) for a supply voltage V_{sup} of −10 V. The p-channel transistor was used as driver for the n-channel load. A gain of 10 was obtained. V_{in}, input voltage; V_{Out}, output voltage.

of charge transport in these organic semiconductors. Measurements on thin-film devices demonstrated a wide variation of the temperature-dependent mobility even for nominally similar preparation conditions, which is ascribed to trap levels, contact effects, and grain boundaries (*4*, *24*). However, it is worth mentioning that these extrinsic defects mainly influence the charge transport in thin films at low temperature. At room temperature, however, similar mobilities as in single crystals can be achieved in pentacene thin films. We prepared pentacene thin films by organic vapor phase deposition on flexible plastic substrates and used them as a basis for FETs, which also revealed ambipolar activity. Growth of large grain (>15 μm) films at elevated temperatures with low grain boundary trap densities seems to be the key parameter for such devices.

The field-effect mobility on single-crystal devices in which the influence of grain boundaries, traps, and residual disorder is minimized (Fig. 5) increases, following a power law from

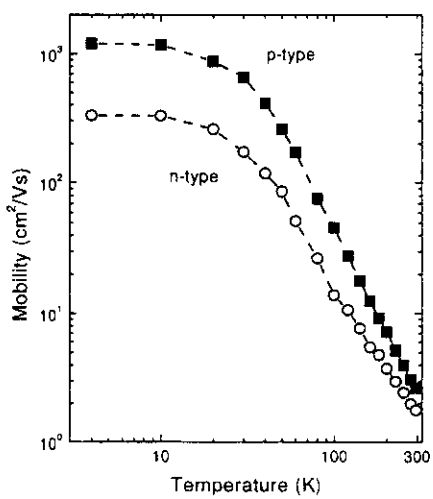

Fig. 5. Temperature dependence of the field-effect mobility of a pentacene single-crystal FET showing a power-law dependence for p-channel as well as for n-channel operation.

2.7 or 1.7 $cm^2\ V^{-1}\ s^{-1}$ at room temperature up to 1200 or 300 $cm^2\ V^{-1}\ s^{-1}$ at low temperatures for holes or electrons, respectively. This temperature dependence and the very high values of the mobility at low temperature suggest that the charge transport is governed by band-like motion rather than by hopping processes. These results are in line with our temperature-dependent space-charge–limited current measurements on pentacene single crystals and also with time-of-flight measurements on naphtalene single crystals (*20*, *25*), where mobilities as high as 400 $cm^2\ V^{-1}\ s^{-1}$ were measured at low temperatures. Therefore, it appears that on a phenomenological level, classical inorganic semiconductor physics may provide an adequate description of charge transport and device performance in polyacene materials.

References and Notes

1. F. Garnier, G. Horowitz, D. Fichou, A. Yassar, *Synth. Met.* **81**, 163 (1996).
2. C. D. Dimitrakopoulos, B. K. Furman, T. Graham, S. Hedge, S. Purushothaman, *Synth. Met.* **92**, 47 (1998).
3. G. Horowitz, *Adv. Mater.* **10**, 365 (1998).
4. H. E. Katz, Z. Bao, A. Dodabalapur, in *Handbook of Oligo- and Polythiophenes*, D. Fichou, Ed. (Wiley-VCH, Weinheim, Germany, 1998), pp. 459–489.
5. S. F. Nelson, Y.-Y. Lin, D. J. Gundlach, T. N. Jackson, *Appl. Phys. Lett.* **72**, 1854 (1998).
6. Y. Y. Lin, D. J. Gundlach, S. F. Nelson, T. N. Jackson, *IEEE Trans. Electron Devices* **44**, 1325 (1997).
7. C. D. Dimitrakopoulos, S. Purushothaman, J. Kymissis, A. Callegari, J. M. Shaw, *Science* **283**, 822 (1999).
8. D. de Leeuw, *Phys. World* (March 1999), p. 31.
9. H. Klauk, D. J. Gundlach, J. A. Nichols, T. N. Jackson, *IEEE Trans. Electron Devices* **46**, 1258 (1999).
10. H. Sirringhaus, N. Tessler, R. H. Friend, *Science* **280**, 1741 (1998).
11. A. Dodabalapur *et al.*, *Appl. Phys. Lett.* **73**, 142 (1998).
12. A. Dodabalapur, H. E. Katz, L. Torsi, R. C. Haddon, *Science* **269**, 1560 (1995).
13. ———, *Appl. Phys. Lett.* **68**, 1108 (1996).
14. A. R. Brown, A. Pomp, C. M. Hart, D. M. de Leeuw, *Science* **270**, 972 (1995).
15. H. Klauk, D. J. Gundlach, T. N. Jackson, *IEEE Electron Devices Lett.* **20**, 289 (1999).
16. C. J. Drury, C. M. J. Mutsaers, C. M. Hart, M. Matters, D. M. de Leeuw, *Appl. Phys. Lett.* **73**, 108 (1998).
17. Y. Y. Lin *et al.*, *Appl. Phys. Lett.* **74**, 2714 (1999).
18. Ch. Kloc, P. G. Simpkins, T. Siegrist, R. A. Laudise, *J. Cryst. Growth* **182**, 416 (1997).
19. J. H. Schön, Ch. Kloc, R. A. Laudise, B. Batlogg, *Phys. Rev. B* **58**, 12952 (1998).
20. S. M. Sze, *Physics of Semiconductor Devices* (Wiley, New York, 1981), p. 442.
21. N. Karl, *Organic Semiconductors*, vol. 17 of *Landolt-Börnstein, New Series, Semiconductors*, O. Madelung, M. Schulz, H. Weiss, Eds. (Springer-Verlag, Berlin 1985), subvolume 17i, pp. 106–218.
22. G. W. Neudeck, H. F. Bare, K. Y. Chung, *IEEE Trans. Electron Devices* **34**, 344 (1987).
23. M. Matsumura and Y. Nara, *J. Appl. Phys.* **51**, 6443 (1980).
24. J. H. Schön and B. Batlogg, *Appl. Phys. Lett.* **74**, 260 (1999).
25. W. Warta and N. Karl, *Phys. Rev. B* **32**, 1172 (1985).

26. One of the authors (J.H.S.) gratefully acknowledges financial support by the Deutsche Forschungsgemeinschaft. Furthermore, we thank E. Bucher for use of equipment and Z. Bao, A. Dodabalapur, H. Katz, and G. A. Thomas for helpful discussions.

27 September 1999; accepted 23 December 1999

24

A Superconducting Field-Effect Switch

J. H. Schön,[1] Ch. Kloc,[1] R. C. Haddon,[2] B. Batlogg[1]

We report here on a novel realization of a field-effect device that allows switching between insulating and superconducting states, which is the widest possible variation of electrical properties of a material. We chose C_{60} as the active material because of its low surface state density and observed superconductivity in alkali metal–doped C_{60}. We induced three electrons per C_{60} molecule in the topmost molecular layer of a crystal with the field-effect device, creating a superconducting switch operating up to 11 kelvin. An insulator was thereby transformed into a superconductor. This technique offers new opportunities for the study of superconductivity as a function of carrier concentration.

The basic idea of an ideal electric "valve" goes back to the late 1920s and involves switching between high- and low-resistance regimes by an applied electric field (*1*). However, reliable devices could not be prepared until 30 years later (*2*), surface states of inorganic semiconductors, such as silicon or germanium, being the major hurdle. Since then, the silicon field-effect transistor (FET) has become the cornerstone of modern semiconductor industry and technology. In addition, there has been an ongoing effort to modulate superconductivity in thin films by an applied static electric field (*3*). Shifts of the transition temperature T_c of up to 30 K have been observed in high-T_c cuprate films, caused by changing the concentration of charge carriers in the electronically active CuO_2 layers (*4*, *5*). However, complete field-induced switching between superconducting and insulating states remains a desirable goal. Here we report on a novel C_{60}-based field-effect device, an ultimate switch between the insulating and superconducting regimes of chemically pure C_{60}.

Working with C_{60} as the starting material is advantageous because so much is known about transport, and ultimately superconductivity, in C_{60} when electrons are induced by chemical doping (*6*, *7*). Undoped C_{60} has a band gap of approximately 2 eV and is therefore insulating, whereas alkali metal–doped C_{60} (A_3C_{60}) exhibits metallic conductivity and, at low temperatures, superconductivity. Furthermore, working with van der Waals–bonded materials, such as molecular crystals, offers the inherent advantage of low surface state densities because of the absence of dangling bond–type surface states. Previous studies on organic semiconductors such as pentacene have shown that in an organic FET the chemical potential can be shifted easily across the band gap of the semiconductor, leading to *n*- as well as *p*-channel activity (*8*).

We have grown C_{60} single crystals that are several mm^3 in size in a stream of hydrogen in an apparatus similar to that used for the growth of other organic semiconductor crystals (*9*). Multiply sublimed material was used as a starting material. In order to prepare field-effect devices on C_{60} single crystals, we evaporated gold source and drain contacts on smooth growth surfaces through a shadow mask. Channels were typically 25 to 50 μm long and 500 to 1000 μm wide. Sputtered Al_2O_3 with a capacitance C_i of 185 nF/cm^2 was used as the gate dielectric. Finally, a gold gate electrode was deposited on top of the oxide (Fig. 1). FET measurements were carried out in vacuum at temperatures between 4 and 300 K. Additional space charge–limited current measurements were used to determine the number of electrically active defects in these high-quality single crystals (*10*). Trap concentrations (deep levels) as low as 3×10^{12} cm^{-3} (one per 5×10^8 C_{60} molecules) are estimated. This level is significantly lower than those reported earlier for other vacuum-grown crystals (*11*).

Previous thin film C_{60} transistors exhibited *n*-type behavior and field-effect mobilities of 0.09 $cm^2/V \cdot s$ (*12*). Figure 1 shows the typical transistor characteristics at room temperature for single-crystal devices. These devices show *n*- as well as *p*-channel activity, reflecting the ambipolar transport in these high-quality single crystals and further emphasizing the low interface state density of the FET. Electron and hole mobilities of 2.1 and 1.8 $cm^2/V \cdot s$, respectively, are deduced from standard semiconductor equations (*13*). At room temperature, the channel resistance can be varied over approximately nine orders of magnitude by the applied gate bias (Fig. 2A). Figure 2A shows the channel resistance as a function of gate charge ($n = C_i V_g / e$, where n is the charge carrier density, C_i is the capacitance, V_g is the gate voltage, and e is the elementary charge) at room temperature and 5 K. The initial drop of the resistance at a few volts reflects the turn-on of the FET. At larger bias, charge accumulates in the channel, leading to a gradual decrease of the resistance. Finally, at very high positive gate voltages, the channel resistance drops abruptly to zero below a critical temperature T_c of 11 K. The channel evidently becomes superconducting. The drop of the resistance depends both on the applied gate voltage and on the temperature. This is shown in Fig. 2B, where the channel resistance is plotted versus temperature and the gate charge. A priori we do not know the electronic nature of the superconducting channel: that is, how many molecular layers become supercon-

[1]Bell Laboratories, Lucent Technologies, 600 Mountain Avenue, Murray Hill, NJ 07974, USA. [2]Departments of Chemistry and Physics and Advanced Carbon Materials Center, University of Kentucky, Lexington, KY 40506, USA.

25

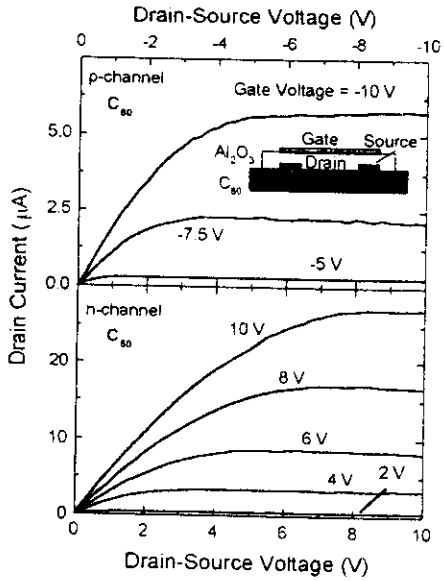

Fig. 1. Source-drain current versus gate voltage at room temperature for a C_{60} single-crystal FET. Top, *p*-channel operation; bottom, *n*-channel operation. The inset shows the schematic structure of a single-crystal FET.

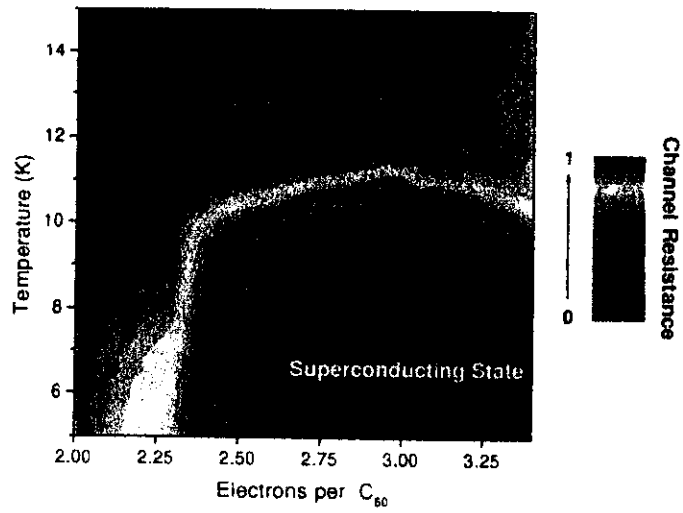

Fig. 3. Channel resistance as a function of temperature and electrons per C_{60} molecule. The electron concentration is calculated assuming that only the first molecular layer accepts charge. The maximum of the transition temperature at three electrons per molecule is in accordance with measurements on chemically doped A_3C_{60} (red, normal state; blue, superconducting state).

ducting. However, excellent agreement with known bulk superconductivity in A_3C_{60} (*14*) is found if we assume that only a single layer of C_{60} molecules accepts the electrons (*15*). The area density is approximately 9×10^{13} C_{60} molecules per cm^2 and the gate charge corresponds to 2.7×10^{13} electrons per cm^2, which is equivalent to three electrons per molecule (C_{60}^{3-}). In bulk A_xC_{60}, this carrier concentration is known to produce the optimum T_c, as the Fermi level lies near the maximum in the density of states of the conduction band. A more detailed map of the superconducting T_c as function of gate bias, expressed in terms of electrons per C_{60}, is shown in Fig. 3. The critical temperature is maximal for three electrons per C_{60} molecule (*14*). Hence, we conclude that field-induced doping results in the same superconducting phenomena as does chemical doping in bulk A_3C_{60}.

Modifying the lattice constant of A_3C_{60} by doping or pressure results in a change of the lattice constant and of the electronic bandwidth, and therefore of the density of states at the Fermi level. Consequently, T_c varies in accordance with Bardeen-Cooper-Schrieffer theory (*6*, *16*, *17*). A systematic variation of T_c with the lattice constant is indeed observed for A_xC_{60} (slight deviations from the cubic crystal structure are ignored here). The value of $T_c = 11$ K observed in our field-effect switch is slightly lower (≈3 to 4 K) than expected from the "universal curve" (Fig. 4). This T_c reduction might be ascribed to the two-dimensional nature of the channel region as compared to the three-dimensional properties of bulk samples (*15*).

A first characterization of the superconducting channel involves the upper critical magnetic field H_{c2} (Fig. 5). The slope of the critical field (dH_{c2}/dT) is approximately −5 T/K in the range reported for bulk A_3C_{60} (*6*). Using the standard extrapolation to $T = 0$ K, we can estimate the coherence length to be on the order of 30 Å. This is further evidence that superconductivity in a C_{60} field-effect device is of the

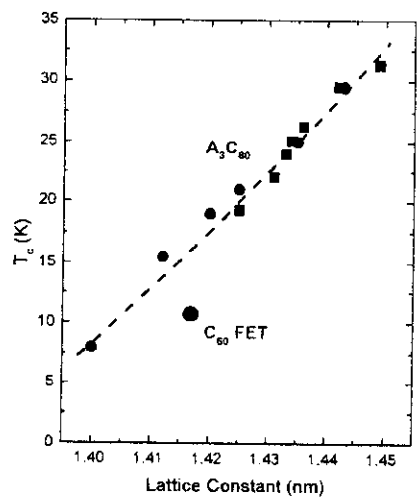

Fig. 4. Transition temperature for bulk alkali-doped A_3C_{60} and our C_{60} field-effect switch. The values for A_3C_{60} are taken from (*6*).

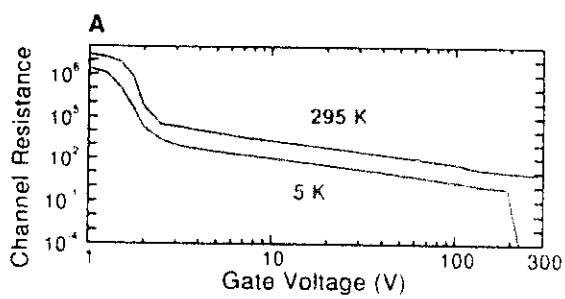

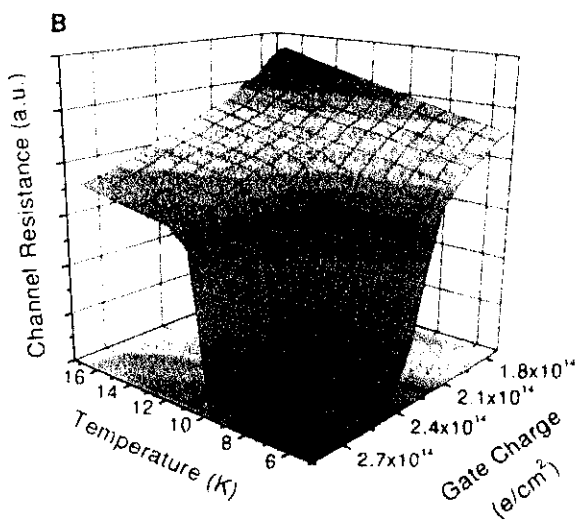

Fig. 2. Channel resistance of a C_{60} single-crystal FET as a function of applied gate voltage and temperature. (**A**) Resistance at 5 K and room temperature as a function of gate voltage. The transition to the superconducting state is seen as a drop in the blue curve. (**B**) Resistance as a function of gate charge (C_iV_g) and temperature, demonstrating superconductivity for concentration above 2.5×10^{14} cm^{-2} and below $T_c = 11$ K.

26

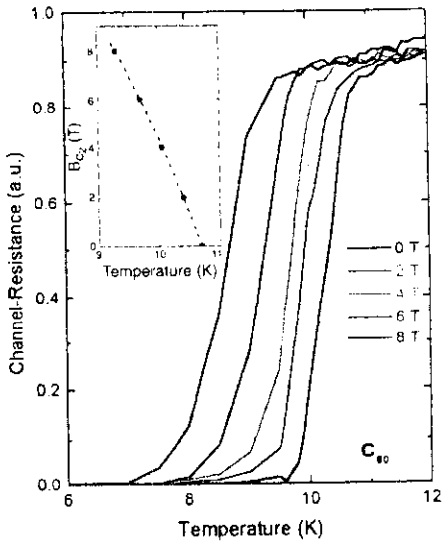

Fig. 5. Transition to the superconducting state for different magnetic fields applied perpendicular to the channel. The variation of the upper critical magnetic field H_{c2} with temperature is shown in the inset (slope ≈ -5 T/K).

same type as in A_3C_{60}. The filling of the band is controlled by the applied gate voltage, and because of the strong electron-phonon interaction in this material, the channel region becomes superconducting below 11 K.

The possibility of investigating superconductivity as function of electron (or hole) density in a simple FET device opens up various opportunities to find superconductivity in new classes of materials, especially organic semiconductors. In addition to being able to implement the longstanding idea of an ultimate field-induced switch (insulator-superconductor transformation), this technique also opens up new ways to substantially modify the electronic state in molecular crystals.

References and Notes

1. J. E. Lilienfeld, U.S. Patent 1,745,175 (1926).
2. M. M. Atalla, E. Tennenbaum, E. J. Scheiber, *Bell Syst. Tech. J.* **28**, 749 (1959).
3. R. E. Glover and M. D. Sherill, *Phys. Rev. Lett.* **5**, 248 (1960).
4. J. Mannhart, J. Ströbel, J. G. Bednorz, Ch. Gerber, *Appl. Phys. Lett.* **62**, 630 (1993).
5. J. Mannhart, J. G. Bednorz, K. A. Müller, D. G. Schlom, J. Ströbel, *J. Alloys Compd.* **195**, 519 (1993).
6. M. S. Dresselhaus, G. Dresselhaus, R. Saito, in *Physical Properties of High Temperature Superconductors IV*, D. M. Ginsberg, Ed. (World Scientific, Singapore, 1994), pp. 471–565; A. P. Ramirez, *Supercond. Rev.* **1**, 1 (1994).
7. A. F. Hebard *et al.*, *Nature* **350**, 600 (1991).
8. J. H. Schön, S. Berg, Ch. Kloc, B. Batlogg, *Science* **287**, 1022 (2000).
9. Ch. Kloc, P. G. Simpkins, T. Siegrist, R. A. Laudise, *J. Cryst. Growth* **182**, 416 (1997).
10. J. H. Schön, Ch. Kloc, R. A. Laudise, B. Batlogg, *Phys. Rev. B* **58**, 12952 (1998).
11. E. Frankevich, Y. Maruyama, H. Ogata, *Chem. Phys. Lett.* **214**, 39 (1993).
12. R. C. Haddon *et al.*, *Appl. Phys. Lett.* **67**, 121 (1995).
13. S. M. Sze, *Physics of Semiconductor Devices* (Wiley, New York, 1981).
14. T. Yildirim *et al.*, *Phys Rev. Lett.* **77**, 167 (1996).
15. It has been observed that the charge transfer across a copper/C_{60} interface also occurs only at the topmost layer of C_{60} [A. F. Hebard, R. R. Ruel, C. B. Eom, *Phys. Rev. B* **54**, 14052 (1996)].
16. C. M. Varma, J. Zaanen, K. Raghavachari, *Science* **254**, 989 (1991).
17. M. A. Schlüter, M. Lannoo, M. Needls, G. A. Baraff, D. Tomanek, *Phys. Rev. Lett.* **68**, 526 (1992).

18. J.H.S. gratefully acknowledges financial support by the Deutsche Forschungsgemeinschaft. We thank E. Bucher for the use of equipment and H. Y. Hwang, D. W. Murphy, H. Störmer, and C. M. Varma for helpful discussions.

6 March 2000; accepted 6 April 2000

27

include the "lab-on-a-chip" concept. The robots could be used for multistation single-cell diagnostics. The robot arm could arrest biological entities (single cells, bacteria, multicellular organisms, etc.) from a sample and then transfer them sequentially to different measurement stations of a multisensor area, as demonstrated by the transfer of the glass bead over the tracks. An array of standing microrobots, whose fingers are treated with adhesion molecules, could be used to select given cells or bacteria in a sample and then transfer them to the multisensor area. The testing could also be done by small additional structures on the microrobot itself, such as extra electrodes for electrical measurements. The electrodes could also be located on the chip itself, for example, in microvials, which also enable single-cell chemical modifications.

A nonbiomedical application for microrobots is the assembly of microstructures in a so-called "factory on a desk." The microrobot could be used to assemble other microstructures. Most of this is still done manually, which is cumbersome, time-consuming, and expensive. Small micromachined conveyors for this purpose have already been demonstrated (*18, 19*). An advantage of assembly in water could be the reduction of gravitational forces and slow diffusion constants of the objects to assemble. The robot could assist the self-assembly (*20*).

Design for the manipulation of cells will require choosing the proper dimensions of the microrobot. The simple scalability of the presented robots—they can easily be reduced in lateral dimension by one order of magnitude—is an important advantage. Also, our microactuators can be seen as active hinges, where only one electrical contact is needed per element, reducing the amount of dead area on the chip. This leads to the possibility of a large number of parallel-operated microrobots on a small area for the simultaneous handling of a large number of cells. Electrostatically operated microactuators require a considerable area for ingenious but complex systems using comb drive actuators and push or pull rods to rotate a plate out of the surface plane. To extend the range of the robot, some modifications of the present design should be made, like adding a rotating base. Using on-chip counter and working electrodes (*21*) would truly integrate the robot into a microelectromechanical system. The operation of such devices may enable new methods in biotechnology.

References and Notes

1. G. Fuhr and S. G. Shirley, *J. Micromech. Microeng.* **5**, 77 (1995).
2. R. Yeh, E. J. J. Kruglick, K. S. J. Pister, *J. Microelectromech. Syst.* **5**, 10 (1996).
3. K. Suzuki, I. Shimoyama, H. Miura, *J. Microelectromech. Syst.* **3**, 4 (1994).
4. C.-J. Kim, A. P. Pisano, R. S. Muller, *J. Microelectromech. Syst.* **1**, 31 (1992).
5. T. Ebefors, J. U. Mattsson, E. Kälvesten, G. Stemme, in *The 10th International Conference on Solid-State Sensors and Actuators, Digest of Technical Papers*, M. Esashi, Ed. (Institute of Electrical Engineers of Japan, Tokyo, 1999), pp. 1202–1205.
6. R. H. Baughman, L. W. Shacklette, R. L. Elsenbaumer, E. J. Plichta, C. Becht, in *Molecular Electronics*, P. I. Lazarev, Ed. (Kluwer Academic, Dordrecht, Netherlands, 1991), pp. 267–289.
7. T. F. Otero and J. M. Sansinena, *Proc. SPIE Int. Soc. Opt. Eng.* **2779**, 365 (1996).
8. A. Della Santa, D. De Rossi, A. Mazzoldi, *Smart Mater. Struct.* **6**, 23 (1997).
9. M. R. Gandhi, P. Murray, G. M. Spinks, G. G. Wallace, *Synth. Met.* **73**, 247 (1995).
10. Q. Pei and O. Inganäs, *Adv. Mater.* **4**, 277 (1992).
11. E. Smela, O. Inganäs, Q. Pei, I. Lundström, *Adv. Mater.* **5**, 630 (1993).
12. E. Smela, O. Inganäs, I. Lundström, *Science* **268**, 1735 (1995).
13. E. W. H. Jager, E. Smela, O. Inganäs, I. Lundström, *Proc. SPIE Int. Soc. Opt. Eng.* **3669**, 377 (1999).
14. E. Smela, *J. Micromech. Microeng.* **9**, 1 (1999).
15. ———, O. Inganäs, I. Lundström, in *The 8th International Conference on Solid-State Sensors and Actuators, and Eurosensors IX, Digest of Technical Papers* (Royal Swedish Academy of Engineering Sciences, Stockholm, 1995), pp. 218–219.
16. A film showing the full movement of this sequence and other actuations of the robotic arm is available at www.sciencemag.org/feature/data/1050465.shl
17. Y. Xia and G. M. Whitesides, *Angew. Chem. Int. Ed. Engl.* **37**, 550 (1998).
18. H. Nakazawa *et al.*, in *The 10th International Conference on Solid-State Sensors and Actuators, Digest of Technical Papers*, M. Esashi, Ed. (Institute of Electrical Engineers of Japan, Tokyo, 1999), pp. 1192–1195.
19. Y. Mita, T. Oba, M. Mita, G. Hashiguchi, H. Fujita, in *The 10th International Conference on Solid-State Sensors and Actuators, Digest of Technical Papers*, M. Esashi, Ed. (Institute of Electrical Engineers of Japan, Tokyo, 1999), pp. 1196–1197.
20. T. L. Breen, J. Tien, S. R. J. Oliver, T. Hadzic, G. M. Whitesides, *Science* **284**, 948 (1999).
21. E. W. H. Jager, E. Smela, O. Inganäs, *Sens. Actuators B Chem.* **56**, 73 (1999).

22. E.W.H.J. is a Ph.D. student in the graduate school Forum Scientum and thanks the Swedish Foundation for Strategic Research (SSF) for its financial support. The micromuscle project is supported by the Swedish Research Council for Engineering Sciences (TFR).

16 March 2000; accepted 2 May 2000

Fractional Quantum Hall Effect in Organic Molecular Semiconductors

J. H. Schön, Ch. Kloc, B. Batlogg

High-quality crystals of the organic molecular semiconductors tetracene and pentacene were used to prepare metal-insulator-semiconductor (MIS) structures exhibiting hole and electron mobilities exceeding 10^4 square centimeters per volt per second. The carrier concentration in the channel region of these ambipolar field-effect devices was controlled by the applied gate voltage. Well-defined Shubnikov–de Haas oscillations and quantized Hall plateaus were observed for two-dimensional carrier densities in the range of 10^{11} per square centimeter. Fractional quantum Hall states were observed in tetracene crystals at temperatures as high as ~2 kelvin.

The quantum Hall effect (QHE) (*1*), in which the Hall resistance R_{xy} of a quasi–two-dimensional (2D) electron or hole gas becomes quantized with values $R_{xy} = h/e^2j$ (where h is Planck's constant, e is the electron charge, and j is an integer), has been observed in a variety of inorganic semiconductors, such as Si, GaAs, InAs, and InP. At higher magnetic fields, fractional quantum Hall states where j is not an integer have also been observed (*2*). A QHE-like state was also seen in organic materials such as Bechgaard salts $(TMTSF)_2X$ (where TMTSF is tetramethyl tetraselenafulvalene and X = ClO_4, ReO_4, or PF_6) (*3–5*). However, in these materials the QHE is related to a series of field-induced spin density wave transitions (*5*) to states with filled Landau bands (*6*). We report on the observation of the integer and fractional QHE in a 2D electron and hole gas in the organic semiconductors tetracene and pentacene. This was achieved in a 2D electron-hole system generated in a single crystal–based MIS device.

Pentacene and tetracene single crystals were grown from the vapor phase in a stream of flowing gas (*7, 8*). The resulting high-quality single crystals support ambipolar (i.e., electron and hole) transport (*9*). Thermally evaporated gold films provide ohmic contacts for holes as well as electrons. Because these crystals are of high resistivity (>10^{14} ohm·cm), the charge carriers must be injected in a field-effect transistor geometry, in which an Al_2O_3 layer (capacitance ~130 nF cm^{-2}) serves as the gate dielectric. A thin gold layer is deposited as the gate electrode on top of the structure. We can then produce a 2D electron or hole gas, respectively, in the channel region of an organic field-effect transistor (*10*), with the carrier density controlled by the gate bias.

The charge transport properties in these

Bell Laboratories, Lucent Technologies, 600 Mountain Avenue, Murray Hill, NJ 07974, USA.

structures were studied down to 1.7 K in magnetic fields up to 9 T by dc measurements in a conventional six-point Hall geometry (Quantum Design physical properties measurement system). A plot of the charge carrier mobility μ as a function of temperature for concentrations of $\sim 10^{11}$ carriers cm^{-2} (Fig. 1) shows that values as high as 10^5 cm^2 V^{-1} s^{-1} are achieved in MIS devices. These electron and hole mobility values are much higher than in earlier generations of crystals on which we had fabricated ambipolar field-effect transistors (*9*). We ascribe this mobility improvement at low temperatures to additional purification and optimization of the growth conditions. Note that the mobilities at higher temperatures remain unchanged, reflecting the intrinsic nature of these high-temperature values (e.g., at room temperature, $\mu_{RT} \approx 3$ cm^2 V^{-1} s^{-1} for holes in pentacene).

The approximate power law dependence of the mobility on temperature ($\propto T^{-n}$, where $n \approx 2.5$ to 2.7) was recognized as the intrinsic property of polyacene single crystals and is ascribed to electron-phonon interaction (*9*, *11*). However, at low temperatures (<10 K), charged point defects seem to limit the mobility (*12*). Hence, careful preparation and purification are prerequisites to obtain mobilities exceeding 10^4 cm^2 V^{-1} s^{-1} in this class of materials.

The magnetoresistance R_{xx} and the Hall resistance R_{xy} at 1.7 K at a fixed magnetic field of 9 T in a single crystalline pentacene MIS device are shown in Fig. 2 as a function of electron and hole density in the transistor channel. Well-pronounced oscillations (Shubnikov–de Haas effect) and Hall plateaus are observed. The Hall plateaus are quantized with $R_{xy} = h/je^2$ (j integer) corresponding to the integer QHE in a 2D electron gas (*1*, *13*). Moreover, the oscillations and plateaus are observed for both electrons and holes in the same sample. Hall plateaus are clearly visible for filling factors $j = 2$ to $j = 6$, and less pronounced structures can be found in R_{xy} up to $j = 10$ (Fig. 3). The effective hole mass m^* can be determined from the temperature-dependent amplitude of the Shubnikov–de Haas oscillations (Fig. 3). We derived values of 1.55 ± 0.2 m_e and 1.3 ± 0.3 m_e (where m_e is the free electron mass) for holes in pentacene and tetracene, respectively. Assuming a cosine-shaped band dispersion and neglecting the in-plane anisotropy, an effective electronic bandwidth W of ~ 0.5 eV can be estimated from this effective mass. This is similar to theoretical estimates based on either local density approximation (*14*) or quantum chemical cluster calculations (*15*), but is much larger than in earlier calculations (*16*, *17*) or estimates based on extended Hückel calculations (*18*).

We observed the most striking results in crystals of tetracene with a low-temperature hole mobility of $\sim 10^5$ cm^2 V^{-1} s^{-1}. By changing the gate voltage, we swept the 2D hole concentration from 0.5 to 5×10^{11} cm^{-2} and simultaneously measured the resistance and Hall voltage. The quantization of both R_{xx} and R_{xy} is well developed (Fig. 4), and the low density renders all the integer quantum Hall states accessible up to $j = 1$. At low densities ($< 7 \times 10^{10}$ cm^{-2}), we can resolve the fractional quantum Hall state $j = 1/3$ and a less pronounced $j = 2/3$, as well as $j = 2/5$ (Fig. 5). This observation is remarkable because it occurs at a relatively high temperature of 1.7 K. This is, however, not too surprising when we consider that the scattering time τ ($\tau = m^*\mu/e$) in our samples ($\mu \approx 10^5$ cm^2 V^{-1} s^{-1}, $m^* \approx 1.5m_e$) is as long as in high-quality GaAs

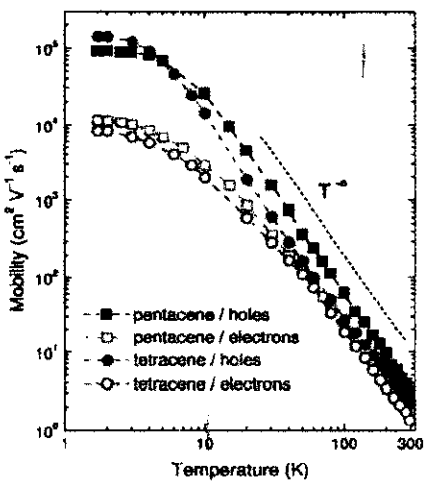

Fig. 1. Charge carrier mobility in pentacene and tetracene as a function of temperature.

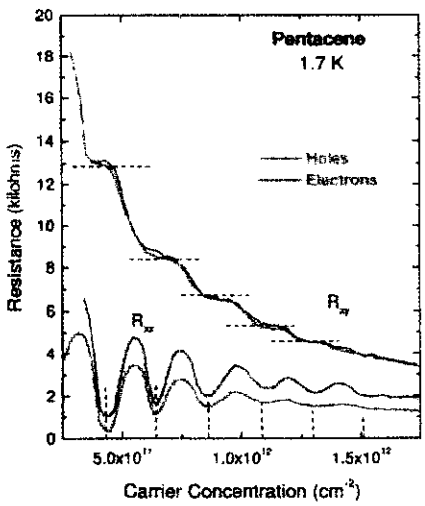

Fig. 2. Magnetoresistance and Hall resistance as function of electron and hole concentration in a pentacene MIS device at 1.7 K. Distinct Hall plateaus and well-pronounced magnetoresistance oscillations are clearly visible.

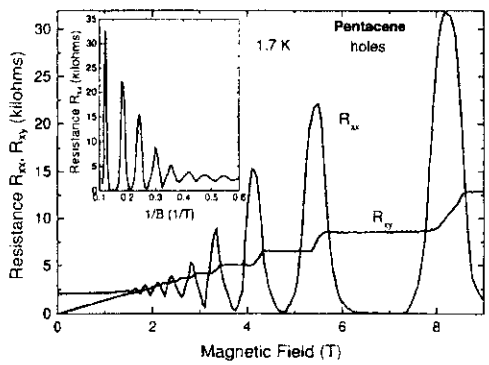

Fig. 3. Shubnikov–de Haas oscillations and quantum Hall plateaus in pentacene at 1.7 K. The hole concentration is 4×10^{11} cm^{-2}. The inset shows the oscillations of the magnetoresistance R_{xx} as function of reciprocal magnetic field. An effective hole mass of $1.55m_e$ is deduced from the temperature dependence of the amplitude of the R_{xx} oscillations.

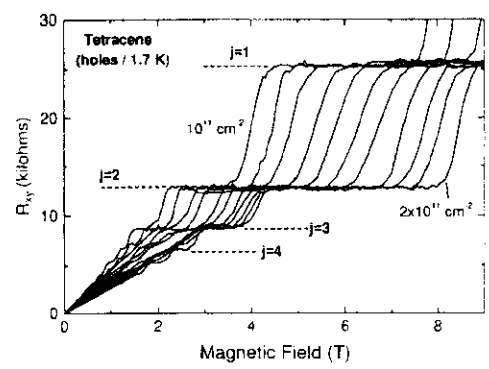

Fig. 4. Hall resistance for different hole concentrations from 10^{11} to 2×10^{11} cm^{-2} in a tetracene MIS device at 1.7 K (step of 10^{10} cm^{-2}). Distinct integer Hall plateaus are observed.

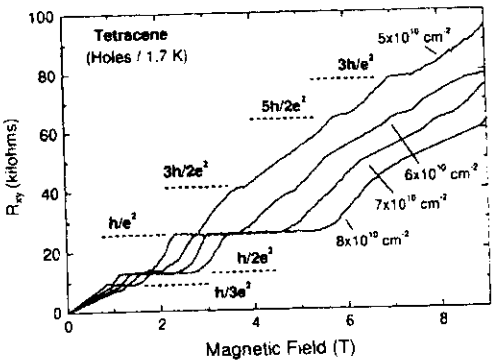

Fig. 5. Hall resistance for low hole concentration (5×10^{10} to 8×10^{10} cm^{-2}) in a tetracene MIS device at 1.7 K. Distinct integer Hall plateaus and the fractional quantum Hall states $j = 1/3$, $j = 2/3$, and $j = 2/5$ are clearly visible.

samples with mobilities of several million square centimeters per volt per second. In addition, the combination of a reduced dielectric constant and a much higher effective mass than in GaAs makes new parameter regions accessible, enabling studies of the physics of strongly interacting electron systems, such as the metal-insulator transition in two dimensions (*19*).

We have presented ample experimental evidence for band-like charge transport in delocalized states in these organic semiconductors: the high mobilities observed at low temperatures, the temperature dependence of the mobility, the large effective bandwidth at low temperatures ($W \gg k_B T$, where k_B is the Boltzmann constant), Shubnikov–de Haas oscillations, and the observation of the integer and fractional QHE. All these observations of transport properties, particularly at low temperatures, are similar to those observed in conventional inorganic semiconductors. It appears that the measured effective masses of order 1 to 1.5 m_e are not those of bare holes or electrons, but instead are charge carriers dressed by a polarization cloud. Looking forward, then, one might expect the adoption of additional concepts from inorganic semiconductor technology (such as superlattices and quantum wells) to yield interesting electronic and optical properties. Layered organic semiconductors (*17, 19, 20*) could offer more latitude for device engineering because they are van der Waals–bonded, and hence minimal constraints are imposed by lattice matching (*21, 22*). Furthermore, interesting new phenomena can be anticipated to result from stronger electron-phonon interaction or strong transport anisotropy, opening up a new field of research.

References and Notes

1. K. von Klitzing, G. Dorda, M. Pepper, *Phys. Rev. Lett.* **45**, 494 (1980).
2. H. L. Stormer, *Rev. Mod. Phys.* **71**, 875 (1999); D. C. Tsui, H. L. Stormer, A. C. Gossard, *Phys. Rev. B* **25**, 1408 (1982).
3. M. Ribault *et al.*, *J. Phys. Lett.* **45**, L935 (1984).
4. R. V. Chamberlin *et al.*, *Phys. Rev. Lett.* **60**, 1189 (1988).
5. P. M. Chaikin, W. Kang, S. Hannahs, R. C. Yu, *Physica B* **177**, 353 (1992).
6. For another organic system, α-(BEDT-TTF)$_2$MHg(SCN)$_4$ salts [where BEDT-TTF is bis(ethylenedithio)-tetrathiafulvalene and M = K or Tl], indirect evidence of a QHE was found in high-field de Haas–van Alphen measurements; this was supported by further evidence from Hall transport measurements. These phenomena in charge-transfer salts, however, are ascribed to a bulk QHE substantially different from the "conventional" QHE in a 2D electron gas in an inorganic heterostructure or in a MIS structure [N. Harrison *et al.*, *Phys. Rev. Lett.* **77**, 1576 (1996); M. M. Honold *et al.*, *Phys. Rev. B* **59**, R10417 (1999)].
7. Ch. Kloc, P. G. Simpkins, T. Siegrist, R. A. Laudise, *J. Cryst. Growth* **182**, 416 (1997).
8. R. A. Laudise, Ch. Kloc, P. G. Simpkins, T. Siegrist, *J. Cryst. Growth* **187**, 449 (1998).
9. J. H. Schön, S. Berg, Ch. Kloc, B. Batlogg, *Science* **287**, 1022 (2000).
10. A. Dodabalapur, L. Torsi, H. E. Katz, *Science* **268**, 270 (1995).
11. N. Karl, J. Marktanner, R. Stehle, W. Warta, *Synth. Met.* **41–43**, 2473 (1991).
12. D. M. Burland and U. Konzelmann, *J. Chem. Phys.* **67**, 319 (1977).
13. K. von Klitzing, *Rev. Mod. Phys.* **58**, 519 (1986).
14. P. M. Littlewood, personal communication.
15. J. Cornil, personal communication.
16. W. Warta and N. Karl, *Phys. Rev. B* **32**, 1172 (1985).
17. D. C. Singh and S. C. Matur, *Mol. Cryst. Liq. Cryst.* **27**, 55 (1974).
18. R. C. Haddon, personal communication.
19. S. V. Kravchenko, G. V. Kravchenko, J. E. Furneaux, V. M. Pudalov, M. D'Iorio, *Phys. Rev. B* **50**, 8039 (1994).
20. H. Akimichi, T. Inoshita, S. Hotta, H. Noge, H. Sakaki, *Appl. Phys. Lett.* **63**, 3158 (1993).
21. T. Minakata and Y. Mori, *Pol. Adv. Technol.* **6**, 611 (1995).
22. F. F. So and S. R. Forrest, *Phys. Rev. Lett.* **66**, 2649 (1991).

23. We thank E. Bucher for use of his equipment, and A. Dodabalapur, J. W. P. Hsu, H. Y. Hwang, H. L. Störmer, and C. M. Varma for helpful discussions. Supported by the Deutsche Forschungsgemeinschaft (J.H.S.).

6 April 2000; accepted 19 May 2000

Discovery of a High-Energy Gamma-Ray–Emitting Persistent Microquasar

Josep M. Paredes,[1]* Josep Martí,[2] Marc Ribó,[1] Maria Massi[3]

Microquasars are stellar x-ray binaries that behave as a scaled-down version of extragalactic quasars. The star LS 5039 is a new microquasar system with apparent persistent ejection of relativistic plasma at a 3-kiloparsec distance from the sun. It may also be associated with a γ-ray source discovered by the Energetic Gamma Ray Experiment Telescope (EGRET) on board the COMPTON–Gamma Ray Observatory satellite. Before the discovery of LS 5039, merely a handful of microquasars had been identified in the Galaxy, and none of them was detected in high-energy γ-rays.

The $V = 11.2$ magnitude star LS 5039 (*1*) has been recently identified as a nearby high-mass x-ray binary with spectral type O7V((f)) (*2*) and persistent radio emission (*3, 4*). Here, we report high-resolution radio observations with the Very Long Baseline Array (VLBA) and the Very Large Array (VLA) that reveal that LS 5039 is resolved into bipolar radio jets emanating from a central core.

[1]Departament d'Astronomia i Meteorologia, Universitat de Barcelona, Av. Diagonal 647, E-08028 Barcelona, Spain. [2]Departamento de Física, Escuela Politécnica Superior, Universidad de Jaén, Calle Virgen de la Cabeza 2, E-23071 Jaén, Spain. [3]Max Planck Institut für Radioastronomie, Auf dem Hügel 69, D-53121 Bonn, Germany.

*To whom correspondence should be addressed. E-mail: josepmp@am.ub.es

Because LS 5039 appeared unresolved ($\leq 0.1''$) to the VLA alone, we proceeded to study this object with milliarc sec resolution using the VLBA at the frequency of 5 GHz (6-cm wavelength) on 8 May 1999. The VLA in its phased array mode, equivalent to a dish of 115-m diameter, also participated as an independent station, providing sensitive baselines with the VLBA antennas. The source 3C345 was used as a fringe-finder, whereas J1733-1304 was the phasing source for the VLA. The data were calibrated using standard procedures in unconnected radio interferometry. The resulting pattern of the observed visibility amplitudes, decaying as a function of baseline length, indicated that LS 5039 had structure at milliarc sec scales.

The final synthesis map (Fig. 1) shows that bipolar jets emerge from a central core. A de-

30